IMMUNOLOGY

IFN-γ–dependent tumor-antigen cross-presentation by lymphatic endothelial cells promotes their killing by T cells and inhibits metastasis

Laure Garnier[1]*, Robert Pick[1]†, Julien Montorfani[1]†, Mengzhu Sun[1], Dale Brighouse[1], Nicolas Liaudet[2], Thomas Kammertoens[3,4], Thomas Blankenstein[3,4,5], Nicolas Page[1,6], Jeremiah Bernier-Latamani[7], Ngoc Lan Tran[1], Tatiana V. Petrova[7], Doron Merkler[1,6,8], Christoph Scheiermann[1,8,9], Stéphanie Hugues[1,8]*

Copyright © 2022 The Authors, some rights reserved; exclusive licensee American Association for the Advancement of Science. No claim to original U.S. Government Works. Distributed under a Creative Commons Attribution NonCommercial License 4.0 (CC BY-NC).

Tumor-associated lymphatic vessels promote metastasis and regulate antitumor immune responses. Here, we assessed the impact of cytotoxic T cells on the local lymphatic vasculature and concomitant tumor dissemination during an antitumor response. Interferon-γ (IFN-γ) released by effector T cells enhanced the expression of immunosuppressive markers by tumor-associated lymphatic endothelial cells (LECs). However, at higher effector T cell densities within the tumor, T cell–based immunotherapies induced LEC apoptosis and decreased tumor lymphatic vessel density. As a consequence, lymphatic flow was impaired, and lymph node metastasis was reduced. Mechanistically, T cell–mediated tumor cell death induced the release of tumor antigens and cross-presentation by tumor LECs, resulting in antigen-specific LEC killing by T cells. When LECs lacked the IFN-γ receptor expression, LEC killing was abrogated, indicating that IFN-γ is indispensable for reducing tumor-associated lymphatic vessel density and drainage. This study provides insight into how cytotoxic T cells modulate tumor lymphatic vessels and may help to improve immunotherapeutic protocols.

INTRODUCTION

Metastasis is the principal cause of mortality in human cancers. Although cancer cells can disseminate through blood vessels (BVs), most solid cancers, such as breast cancer and melanoma, propagate through the lymphatic vessels (LVs) to first reach the sentinel lymph nodes (LNs) (*1*). Occurrence of tumor cells in LNs is associated with poor prognosis in multiple types of cancers (*2*). Studies have shown that metastatic tumor cells additionally migrate through LVs to settle adjacent LNs, where they invade local BVs to further colonize distant organs (*3*, *4*). Tumor LVs are not simple passive conduits for metastatic dissemination. Mouse and human studies indicate that lymphatic endothelial cells (LECs) lining the lymphatic vasculature react to factors present in the tumor microenvironment (TME), promoting LV growth and remodeling in primary tumors and draining LNs (dLNs). This process is called lymphangiogenesis and correlates with metastasis and impaired disease-free survival (*2*, *5*). Expression of the lymphangiogenic factor vascular endothelial growth factor-C (VEGF-C) in patient samples is associated with LN metastasis in several types of cancers (*2*, *6*, *7*). In murine models, alterations of VEGF-C and VEGF-D receptor signaling influence metastatic dissemination to LNs and/or distal organs (*8*–*16*). LV expansion within sentinel LNs induces the formation of a "premetastatic niche" that would favor metastatic cell colonization (*10*, *17*, *18*). LVs in distant metastatic regions further contribute to tumor progression by attracting chemotherapy-resistant cancer stem-like cells (*19*). Moreover, LVs promote lung metastasis and additional spreading to other organs in an inducible lung lymphangiogenesis mouse model (*20*). In patients with melanoma, lymphatic exudates are enriched in tumor-derived factors and exhibit distinct tumor protein profiles depending on the metastatic stage of the patients, suggesting that they might be used to predict disease progression and response to treatment (*21*).

Besides their critical role in tumor cell dissemination, LVs are key players in the initiation and the regulation of antitumor immune responses, including T cell activation and infiltration in tumors. While studies have indicated a possible local priming of naïve T cell infiltrating solid tumors (*22*–*24*), antigen transport by dendritic cells (DCs) through LVs to the dLNs is, nevertheless, crucial for the initiation of T cell responses in melanoma (*25*, *26*). Consistent with a beneficial role of the lymphatic vasculature in antitumor immunity, the expression of genes associated to lymphatics or LV density (LVD) positively correlates with tumor-infiltrating inflammatory immune cell numbers in primary colorectal cancer and melanoma (*27*–*29*). Transgenic mice lacking or exhibiting disturbed local LVs demonstrate limited tumor drainage, reduced DC migration to dLNs, decreased tumor-infiltrating leucocyte numbers, and impaired antitumor adaptive immunity (*25*, *30*). However, LVD and lymphatic score (attributed by the relative expression levels of LV-related genes) are also associated with enhanced infiltration of immunosuppressive cells and expression of immunoregulatory molecules (*25*, *27*, *28*). Therefore, although LVs are required for intratumoral T cell infiltration, they inhibit ongoing adaptive antitumor immunity. In mouse

[1]Department of Pathology and Immunology, Geneva Medical School, Geneva, Switzerland. [2]Bioimaging Core Facility, Faculty of Medicine, University of Geneva, Geneva, Switzerland. [3]Institute of Immunology, Charité Campus Buch, 13125 Berlin, Germany. [4]Max Delbrück Center for Molecular Medicine, 13125 Berlin, Germany. [5]Berlin Institute of Health, 10117 Berlin, Germany. [6]Department of Pathology and Immunology, Division of Clinical Pathology, University of Geneva and University Hospital of Geneva, Geneva, Switzerland. [7]Department of Fundamental Oncology, Ludwig Institute for Cancer Research and Division of Experimental Pathology, University of Lausanne and University of Lausanne Hospital, 1066 Lausanne, Switzerland. [8]Geneva Centre for Inflammation Research, Geneva, Switzerland. [9]Walter-Brendel-Centre of Experimental Medicine, BioMedical Centre, Ludwig Maximilians University Munich, Planegg-Martinsried, Germany.
*Corresponding author. Email: stephanie.hugues@unige.ch (S.H.); laure.garnier@unige.ch (L.G.)
†These authors contributed equally to this work.

melanoma, tumor dLN (TdLN) LECs cross-present tumor antigen to foster the apoptosis of tumor-specific $CD8^+$ T cells (*31*). In colorectal cancer, VEGF-C signaling in tumor LECs enhances their immunosuppressive properties through a synergistic cooperation with tumor-associated macrophages (*32*). In multiple subcutaneous tumor mouse models, tumor LECs up-regulate the immunosuppressive molecule programmed death-ligand 1 (PD-L1) in response to interferon-γ (IFN-γ) produced by tumor-specific $CD8^+$ T cells (*33*, *34*), thereby reducing intratumoral $CD8^+$ T cells (*34*). Recently, we demonstrated that IFN-γ signaling induces the up-regulation of major histocompatibility complex (MHC) class II molecules by tumor LECs, which locally promote the suppressive functions of regulatory T cells, leading to an inhibition of cytotoxic $CD8^+$ T lymphocyte (CTL) effector functions and promoting tumor growth (*35*). VEGF-C–induced lymphangiogenesis combined with immunotherapy can potentiate antitumor T cell responses in murine melanoma and glioblastoma (*28*, *36*). Furthermore, serum VEGF-C levels in patients with melanoma positively correlate with a response to immunotherapy and progression-free survival (*28*). In agreement, lymphangiogenic vaccines composed of irradiated tumor cells engineered to overexpress VEGF-C administered outside the tumor bed promote tumor-specific T cell immunity and potentiate anti–programmed cell death protein 1 (PD-1) immunotherapy in mouse melanoma (*37*).

Although the dual role and the spatiotemporal effects of LVs in antitumor immunity need to be considered, targeting the lymphatic vasculature represents a promising therapeutic strategy to restrain cancer cell dissemination. A better understanding of the mechanisms implicated in solid tumor rejection and disruption of the tumor vasculature will help to optimize immunotherapeutic protocols. Effective antigen-dependent killing of stromal cells by transferred CTLs is crucial to indirectly eliminate antigen loss variants (ALVs) in established tumor (*38*, *39*). Cancer cell death enhances the elimination of the tumor stroma through the release of tumor antigens that sensitize stromal cells for antigen-specific CTL killing (*38*–*40*). Tumor necrosis factor (TNF), Fas ligand (FasL), and IFN-γ expression by CTLs—together with the expression of their respective receptors TNFR, Fas, and IFN-γR by stromal cells—are required for the bystander eradication of ALVs (*41*–*43*). IFN-γ produced by adoptively transferred CTLs inhibits tumor-induced angiogenesis (*44*). The selective expression of IFN-γR by endothelial cells is sufficient for IFN-γ–induced BV destruction and tumor regression (*45*). IFN-γ secretion by T cells reduces LVD in both steady-state and inflamed LNs (*46*) and promotes LEC immunosuppressive function in tumors (*34*, *35*). However, the impact of T cell–based immunotherapies on intratumor LVD has not been determined.

In this study, we show that therapies involving cytotoxic T cell responses targeting tumors induce LEC apoptosis and lead to a reduction of tumor LVD. As a consequence, lymphatic flow drainage and metastatic dissemination into LNs are diminished. These effects are abolished in the absence of IFN-γR expression by LECs, indicating that T cells rely on the IFN-γ signaling pathway to restrain tumor LVs. Mechanistically, IFN-γ signaling in LECs potentiates their capacity to cross-present tumor antigens released after CTL-mediated tumor cell death and their subsequent killing by CTLs. This study provides important insights into how CTLs modulate LVs to optimize the design of protocols for immunotherapies in cancer.

RESULTS

Immunotherapy using tumor-specific $CD8^+$ T cells induces tumor LEC apoptosis

We used several approaches to evaluate how T cell–based immunotherapies affect tumor LECs. First, we adoptively transferred 1×10^6 ovalbumin (OVA)–specific T cell receptor (TCR) transgenic OT-1 $CD45.1^+$ $CD8^+$ effector T cells into B16F10-OVA^+VC^+ tumor-bearing C57BL/6 mice (Fig. 1A). B16F10-OVA^+VC^+ is a melanoma cell line expressing the model antigen OVA and engineered to produce elevated levels of the lymphangiogenic factor VEGF-C (*31*). OT-1 effectors efficiently infiltrated OVA-expressing tumors, where they actively produced IFN-γ and granzyme-B (fig. S1A). OT-1 transfer induced efficient tumor regression (Fig. 1A), as well as a significant up-regulation of PD-L1 and MHCII molecules by tumor LECs (fig. S1, B and C), corroborating earlier findings that LECs exposed to IFN-γ up-regulated IFN-γ–target genes (*34*, *35*). In addition, OT-1 effector cell transfer resulted in a significant decrease in the density of tumor LECs (Fig. 1B), as well as their increased expression of the proapoptotic marker activated caspase 3 (cleaved casp-3) (Fig. 1C). In contrast, we did not observe any effect of OT-1 transfer on LEC proliferation (fig. S1D), indicating that elevated intratumoral VEGF-C levels were maintained following OT-1–mediated tumor cell killing. In vitro generated OT-1 effectors adoptively transferred into tumor-bearing mice, representing 2% of $CD8^+$ T cells in TdLNs (fig. S1E), and failed at inducting cleaved casp-3 in LN LECs (fig. S1F).

Tumor LV reduction and tumor LEC apoptosis were also observed when OT-1 effector cells were adoptively transferred into mice bearing a mixed tumor, resulting from the injection of a 9:1 B16F10-VC^+ and B16F10-OVA^+VC^+ cell ratio (fig. S1, G to I). Tumor rejection was not observed in this context (fig. S1G), ruling out the possibility that reduced LV densities in tumors following OT-1 effector cell transfer resulted from lower VEGF-C levels in smaller tumors. We further performed LEC (Lyve-1^+) (*31*, *35*) and OT-1 ($CD45.1^+$) immunofluorescent staining on tumors from B16F10-OVA^+VC^+–bearing mice adoptively transferred with OT-1 effector cells (+OT-1) or not (–). OT-1 transfer induced a decrease in LV area (Lyve-1^+) (Fig. 1D), with a more pronounced effect on LVs located at the center of the tumor compared to the periphery of the tumor (Fig. 1D). OT-1 transfer was further associated with a higher proportion of cleaved casp-3^+ cells on tumor LECs (Fig. 1E). Transferred OT-1 cells were not randomly distributed in tumors but were preferentially localized in close proximity of tumor LVs (fig. S1J).

We next vaccinated B16F10-OVA^+VC^+ tumor-bearing mice with CpG-B + OVA, which led to increased density of IFN-γ– and granzyme-B–producing $CD8^+$ T cell in the tumor (fig. S2A), tumor regression (Fig. 1F), as well as enhanced expression levels of PD-L1 and MHCII on tumor LECs (fig. S2, B and C). LEC proliferation was slightly decreased upon vaccination (fig. S2D). LVD was significantly reduced 7 days after vaccination (Fig. 1G), and cleaved casp-3 was increased in tumor LECs (Fig. 1H). To determine whether the pathway can be observed by vaccinating with an endogenous tumor antigen, B16F10-OVA^+VC^+ tumor-bearing mice were vaccinated with CpG-B + Gp100 peptide and transferred with Gp100-specific TCR transgenic Pmel-1 $CD8^+$ T cell effectors. Gp100 vaccination, Pmel-1 transfer, or a combination of the two all induced tumor regression and up-regulation of PD-L1 and MHCII by tumor LECs (fig. S3, A to C). However, only the combination of vaccination and T cell transfer reduced tumor LVD (fig. S3D) and enhanced LEC apoptosis (fig. S3E), confirming our observations by using an

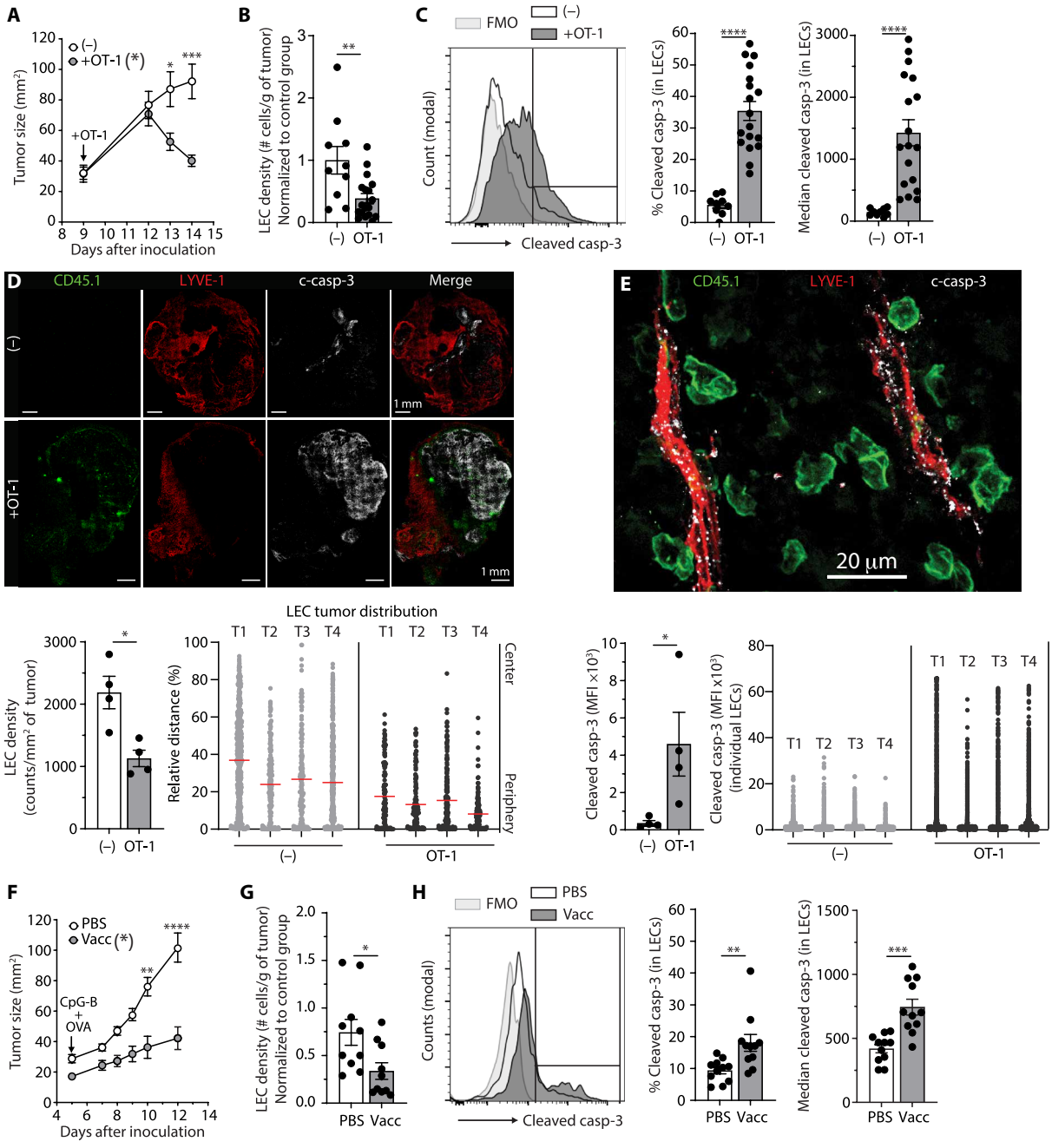

Fig. 1. Boosting tumor-specific T cell responses promotes tumor LEC apoptosis. (**A** to **E**) C57BL/6 mice were injected or not with in vitro activated CD8$^+$ OT-1 CD45.1$^+$ cells (1×10^6 cells) 9 days after B16F10-OVA$^+$VC$^+$ inoculation. (A) Tumor growth. (B) LVD (number of LECs per grams of tumor, normalized to control group) and (C) frequency and median of cleaved casp-3$^+$ (casp-3) LECs (CD45^{neg} CD31$^+$ GP38$^+$) in tumors at day 14 by flow cytometry. Graphs represent a pool of two experiments with 10 to 18 mice per group. (D and E) Representative immunofluorescent labeled tumor sections stained against OT-1 (CD45.1; green), LECs (Lyve-1; red), cleaved casp-3 (c-casp-3) (white), and merge without (–) or upon OT-1 transfer at day 4 after transfer. (D) LVD measured as Lyve-1$^+$ cell counts per square millimeter of tumor and relative tumor LEC distribution in individual tumors (T1 to T4). (E) LEC cleaved casp-3 activity [mean fluorescence intensity (MFI)] per tumor and per individual tumor LECs. (**F** to **H**) C57BL/6 mice were vaccinated or not with CpG-B + OVA at day 5 after B16F10-OVA$^+$VC$^+$ inoculation. (F) Tumor growth. (G) LVD and (H) frequency and median of cleaved casp-3$^+$ LECs in tumors at day 12 by flow cytometry. Graphs represent a pool of two experiments with 10 to 11 mice per group. (A and F) Two-way analysis of variance (ANOVA) test; (B to E, G, and H) Mann-Whitney test. Error bars show means ± SEM. *P < 0.05, **P < 0.01, ***P < 0.001, ****P < 0.0001.

endogenous tumor antigen. Last, B16F10-VC$^+$ (OVA negative) tumor-bearing mice were vaccinated with irradiated B16F10-VC$^+$ cells in the presence of CpG-B and adoptively transferred with CD8$^+$ T cells preactivated in vitro with irradiated B16F10-VC$^+$ cells loaded DCs (Polyclonal-ATT). This treatment induced a potent tumor growth control (fig. S3F), induced the up-regulation of MHCII by tumor LECs (fig. S3G), and resulted in reduced tumor LEC density (fig. S3H) and increased frequencies of cleaved casp-3$^+$ LECs (fig. S3I).

Therefore, tumor LEC killing and LV inhibition can be induced by boosting polyclonal tumor-specific CTLs. Together, our data indicate that immunotherapies aiming at increasing the numbers of tumor-specific T cell effectors in tumors locally induce LEC apoptosis and decrease LVD.

Tumor LEC apoptosis requires elevated CTL numbers

We hypothesized that a threshold of CTL density in tumors is necessary to overcome IFN-γ–mediated LV immunosuppression through the killing of tumor LECs. To determine whether LEC killing correlates with CTL density, we transferred two different amounts (0.05×10^6 and 0.5×10^6) of OT-1 effectors in B16F10-OVA$^+$VC$^+$ tumor-bearing mice. We observed a dose-dependent reduction of tumor growth 5 days after T cell transfer (Fig. 2A), which was correlated with the density of IFN-γ– and granzyme-B–producing OT-1 cell in tumors (fig. S4A). Whereas both doses induced PD-L1 up-regulation by tumor LECs as soon as 3 days after T cell transfer (fig. S4B), increased frequencies of cleaved casp-3$^+$ LECs (Fig. 2B) and reduced LEC densities (Fig. 2C) happened to be T cell dose dependent. Densities of OT1 T cells within the tumor (Fig. 2D), producing IFN-γ (Fig. 2E) and granzyme-B (Fig. 2F), were positively correlated to the frequency of apoptotic tumor LECs, reinforcing a dose-dependent effect of OT-1 effectors on tumor LEC apoptosis. However, given the data distribution observed in Fig. 2 (D to F), additional factors present in the TME likely influence OT-1 effector location and functions.

We next investigated whether tumor LEC killing also occurs in the absence of immunotherapy in a more immunogenic tumor mouse model. We used MC38-OVA$^+$ adenocarcinoma cells engineered to overproduce VEGF-C (MC38-OVA$^+$VC$^+$ cells). In vitro, VEGF-C mRNA levels in MC38-OVA$^+$VC$^+$ cell cultures were increased around 60-fold compared with the MC38-OVA cell line and were 1.6-fold less than in B16F10-OVA$^+$VC$^+$ cells (fig. S4C). In vivo, VEGF-C levels in B16F10-OVA$^+$VC$^+$ and MC38-OVA$^+$VC$^+$ tumors were measured in the same range of concentrations (fig. S4D). We compared C57BL/6 inoculated with either B16F10-OVA$^+$VC$^+$ cells or MC38-OVA$^+$VC$^+$ cells. MC38-OVA$^+$VC$^+$ tumors exhibited a slower growth (fig. S4E). Granzyme-B CD8$^+$ effector T cell densities were significantly enhanced in MC38-OVA$^+$VC$^+$ tumors compared to B16F10-OVA$^+$VC$^+$ tumors (fig. S4F). PD-L1 expression levels were increased in MC38-OVA$^+$VC$^+$ compared to B16F10-OVA$^+$VC$^+$ tumor LECs (fig. S4G). LV frequency and density were markedly lower (fig. S4H), and the frequency of cleaved casp-3 in tumor LECs was enhanced in MC38-OVA$^+$VC$^+$ tumors (fig. S4I). Although different molecular and/or cellular actors specific to a given TME may also influence LEC density, these data show that elevated CTL numbers in the tumor tissue correlate with tumor LVD inhibition. We next thought to determine whether LEC killing by infiltrating CTLs occurs in B16F10-OVA$^+$ tumors, which do not overexpress VEGF-C. OT-1 effector transferred in B16F10-OVA$^+$ and B16F10-OVA$^+$VC$^+$ tumor-bearing mice controlled tumor growth (fig. S4J) and induced PD-L1 and MHCII up-regulation in tumor LECs (fig. S4, K and L). Frequencies of cleaved casp-3$^+$ LECs were notably elevated in B16F10-OVA$^+$ tumors compared to B16F10-OVA$^+$VC$^+$ tumors already in the absence of OT-1 transfer (fig. S4M). As expected, OT-1 transfer significantly increased cleaved casp-3$^+$ LEC frequencies (fig. S4M) and reduced LEC densities (fig. S4N) in B16F10-OVA$^+$VC$^+$ tumors. In contrast, cleaved casp-3$^+$ LEC frequencies remained similar in

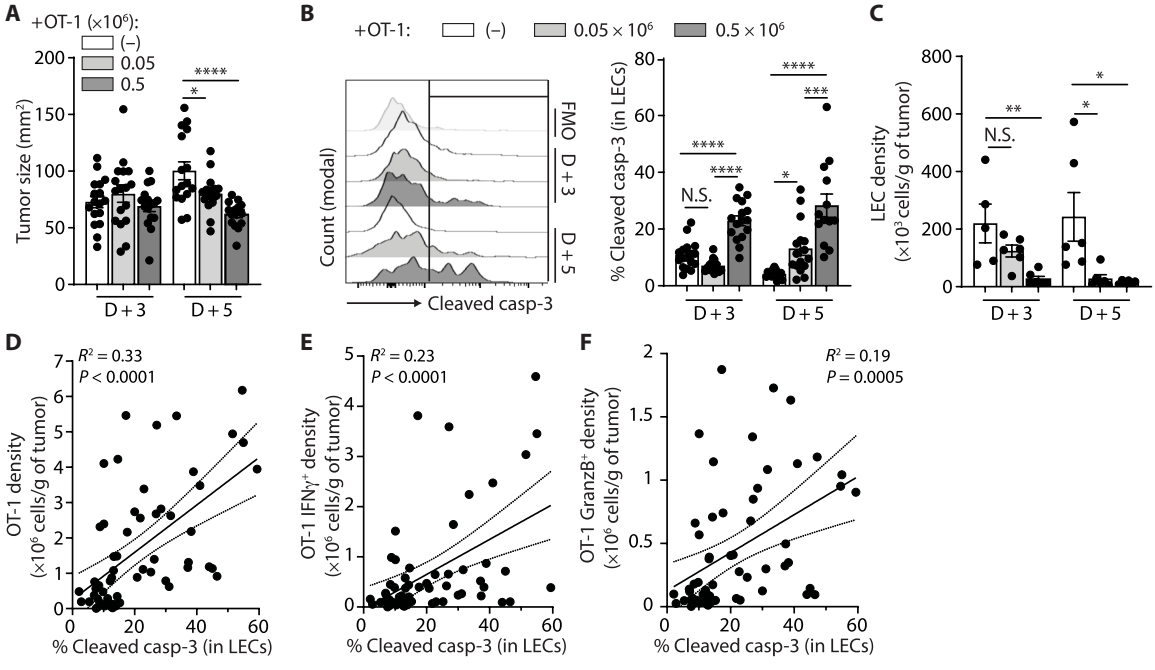

Fig. 2. Positive correlation between intratumoral CTL densities and tumor LEC killing. (**A** to **C**) C57BL/6 mice were injected or not with different doses of in vitro activated OT-1 cells (0.05×10^6 or 0.5×10^6 cells) 9 days after B16-OVA-VC inoculation and euthanized 3 or 5 days later. (A) Tumor size, (B) frequency of cleaved casp-3$^+$ tumor LECs, and (C) LEC density 3 and 5 days after injection. Data represent a pool of three experiments (A and B) with $N = 16$ to 17 mice per group and one experiment (C) with 5 to 6 mice per group. (**D** to **F**) Correlations between (D) OT-1, (E) OT-1–producing IFN-γ, and (F) OT-1–producing granzyme-B densities and the frequency of cleaved casp-3$^+$ tumor LECs 5 days after transfer of 0.5×10^6 activated OT-1 cells. Data represent a pool of six experiments, $N = 59$ mice. (A to C) One-way ANOVA test; (D to F) linear regression. Error bars show means ± SEM. N.S., not significant. *$P < 0.05$, **$P < 0.01$, ***$P < 0.001$, ****$P < 0.0001$.

B16F10-OVA$^+$ tumors with and without OT-1 transfer (fig. S4M). The amount of LECs is extremely low in B16F10-OVA$^+$ compared to B16F10-OVA$^+$VC$^+$ tumors (fig. S4N), supporting the idea that an elevated ratio CTL/LEC results in tumor LEC killing by infiltrating CTLs. Accordingly, whereas the density of CTL was 10-fold higher in B16F10-OVA$^+$VC$^+$ tumors compared to B16F10-OVA$^+$ tumors (fig. S4O), the ratio CTL density/LEC density remained 50-fold higher in B16F10-OVA$^+$ tumors compared to B16F10-OVA$^+$VC$^+$ tumors (fig. S4P).

Adoptive transfer of tumor-specific T cells restricts lymphatic drainage

LVs are the primary route for cancer cell spreading and metastasis establishment in sentinel LNs and distal organs. Therefore, targeting the lymphatic vasculature represents a promising therapeutic strategy to restrain cancer cell dissemination. We next assessed whether LVD decrease upon tumor-specific CD8$^+$ T effector transfer would result in impaired LV drainage functions.

In B16F10-OVA$^+$VC$^+$ tumor-bearing mice injected intratumorally with fluorescein isothiocyanate (FITC) beads, the migration of FITC$^+$ DCs in TdLNs was reduced in mice adoptively transferred 5 days before with 0.5×10^6 but not 0.05×10^6 of OT-1 effectors (Fig. 3A). In contrast, the frequency of total DCs in the TdLNs was not altered in mice adoptively transferred with either of the two OT-1 doses (Fig. 3B). In addition, the transfer of 0.5×10^6 OT-1 cells reduced metastasis in LNs proximal to the tumor, as quantified by the black color intensity in inguinal, axillary, and brachial LNs (fig. S5A). Whereas the number of cancer-positive inguinal LNs was not affected by OT-1 transfer, we observed an increased proportion of axillary and brachial LNs devoid of metastasis following adoptive T cell transfer (ATT) (fig. S5A). Gp100 staining of TdLN sections further indicated that LN metastasis was significantly reduced 5 days after the transfer of 0.5×10^6 OT-1 effectors, in terms of both the number of metastatic foci per LNs and the number of metastasis-positive LNs (fig. S5B). The size of primary tumors being significantly decreased upon OT-1 adoptive transfer, reduced LN metastasis can be a combination of lower tumor cell spreading and impaired LV drainage. Therefore, we next thought to determine whether LV disruption significantly contributes to reduced LN metastasis following ATT. We adoptively transferred OT-1 cells in B16F10-OVA$^+$VC$^+$ tumor-bearing mice and further injected peritumorally cell trace violet (CTV)–labeled B16F10-VC$^+$ tumor cells at a time point primary tumor sizes were not decreased by the adoptive transfer of OT1. Adoptive transfer of OT-1 cells drastically inhibited the de novo migration of CTV-labeled B16F10-VC$^+$ tumor cells toward primary and secondary TdLNs (Fig. 3C). In summary, these results demonstrate that elevated numbers of tumor-specific effector T cells induce LEC apoptosis in tumors, resulting in LV dismantling, altered drainage to TdLNs, and diminished LN metastasis.

ATT-mediated dismantling of tumor LV and LN metastasis inhibition are dependent on IFN-γR signaling in LECs

IFN-γ has been shown to negatively affect LN-LV (*46*). As CTLs represent a substantial source of IFN-γ in tumors, we next sought to determine whether LV destruction by ATT relies on IFN-γR signaling in tumor LECs. We generated conditional knockout (KO) mice in which LECs do not express IFN-γR subunit 2. Prox-1 Cre^{ERT2} mice (*47*), which express the tamoxifen-inducible Cre recombinase under the promoter of the LEC-specific transcription factor Prox-1, were crossed with IFN-γR2$^{flox/flox}$ mice (IFN-γR$^{\Delta prox\text{-}1}$ mice) (*48*). We validated by quantitative polymerase chain reaction (qPCR) the

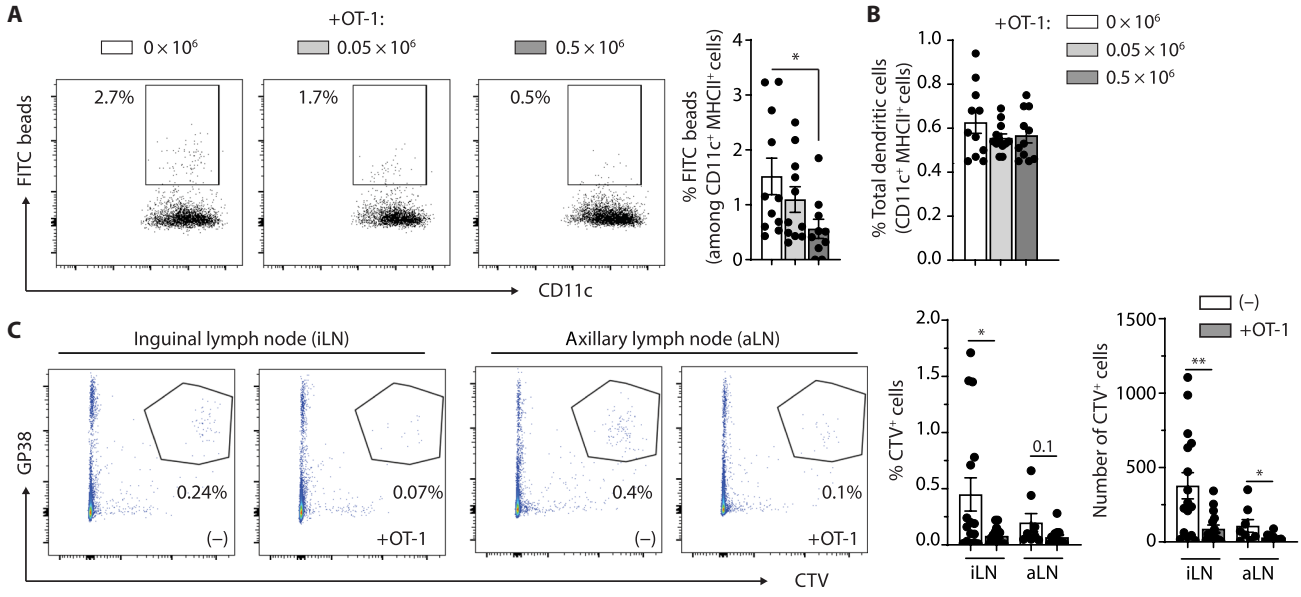

Fig. 3. Tumor LV drainage functions are impaired upon adoptive T cell transfer. (**A** and **B**) C57BL/6 mice were injected or not with different doses of in vitro activated OT-1 cells (0.05×10^6 or 0.5×10^6 cells) 9 days after B16F10-OVA$^+$VC$^+$ inoculation and euthanized 5 days later. FITC-labeled beads (0.5 mm) were injected intratumorally 24 hours before euthanasia. Frequencies of (A) FITC beads$^+$ DCs (CD11c$^+$MHCII$^+$) and (B) total DCs in TdLNs (pool of inguinal and axillary LN) by flow cytometry. Data represent two pooled experiments, $N = 10$ to 11 mice per group. (**C**) C57BL/6 mice were inoculated with B16F10-OVA$^+$VC$^+$ and were injected or not with 0.5×10^6 in vitro activated OT-1 cells 9 days later. CTV-labeled B16F10-VC$^+$ tumor cells were injected peritumorally at day 13, and mice were euthanized at day 14. Frequencies of GP38$^+$ CTV$^+$ cells in the TdLNs (inguinal and axillary). Data represent a pool of three experiments, $N = 14$ to 15 mice per group. (A and B) One-way ANOVA; (C) Mann-Whitney statistical test. Error bars show means ± SEM. *$P < 0.05$, **$P < 0.01$.

deletion of IFN-γR2 in LECs sorted from B16F10-OVA^{+}VC^{+} tumors of IFN-γR$^{\Delta prox\text{-}1}$ mice (fig. S6A). Lyve-1 staining of naïve LNs showed a modest but significant increase in LVD in steady-state IFN-γR$^{\Delta prox\text{-}1}$ LNs compared to IFN-γR^{WT} control LNs (Fig. 4A), confirming previously published data that T cell–derived IFN-γ secretion inhibits LV-specific genes in LN LECs and consequently reduce in LN-LV (*46*). Whereas ATT did not modify IFN-γR1 and Jak1 mRNA levels, it enhanced the expression of STAT-1 and different IFN-γ response genes, such as IFN regulatory factor 1 (IRF-1), CIITA (Class II Major Histocompatibility Complex Transactivator), MHCII, and PD-L1 genes in LECs from B16F10-OVA^{+}VC^{+} tumors in IFN-γR^{WT} control mice (fig. S6A). These effects were abolished in tumor LECs from IFN-γR$^{\Delta prox\text{-}1}$ mice, highlighting an IFN-γR signaling–dependent mechanism (fig. S6A). PD-L1 and MHCII were also up-regulated at the protein level in tumor LECs following OT-1 transfer in IFN-γR^{WT} controls, whereas it was abrogated in IFN-γR$^{\Delta prox\text{-}1}$ mice (fig. S6, B and C). Notably, PD-L1 and MHCII up-regulation after OT-1 transfer was observed in tumor blood endothelial cells (BECs) from both IFN-γR^{WT} and IFN-γR$^{\Delta prox\text{-}1}$ mice (fig. S6, D and E), again validating the specific deletion of IFN-γR in LECs.

Although OT-1 transfer similarly induced B16F10-OVA^{+}VC^{+} tumor regression in IFN-γR^{WT} and IFN-γR$^{\Delta prox\text{-}1}$ mice (Fig. 4B), both the reduction of tumor LVD (Fig. 4C) and the increase of LEC apoptosis (Fig. 4D) induced by ATT were abolished in IFN-γR$^{\Delta prox\text{-}1}$ mice, demonstrating that IFN-γ is crucial for LV killing. Whereas LVs were increased in steady-state LNs from IFN-γR$^{\Delta prox\text{-}1}$ mice

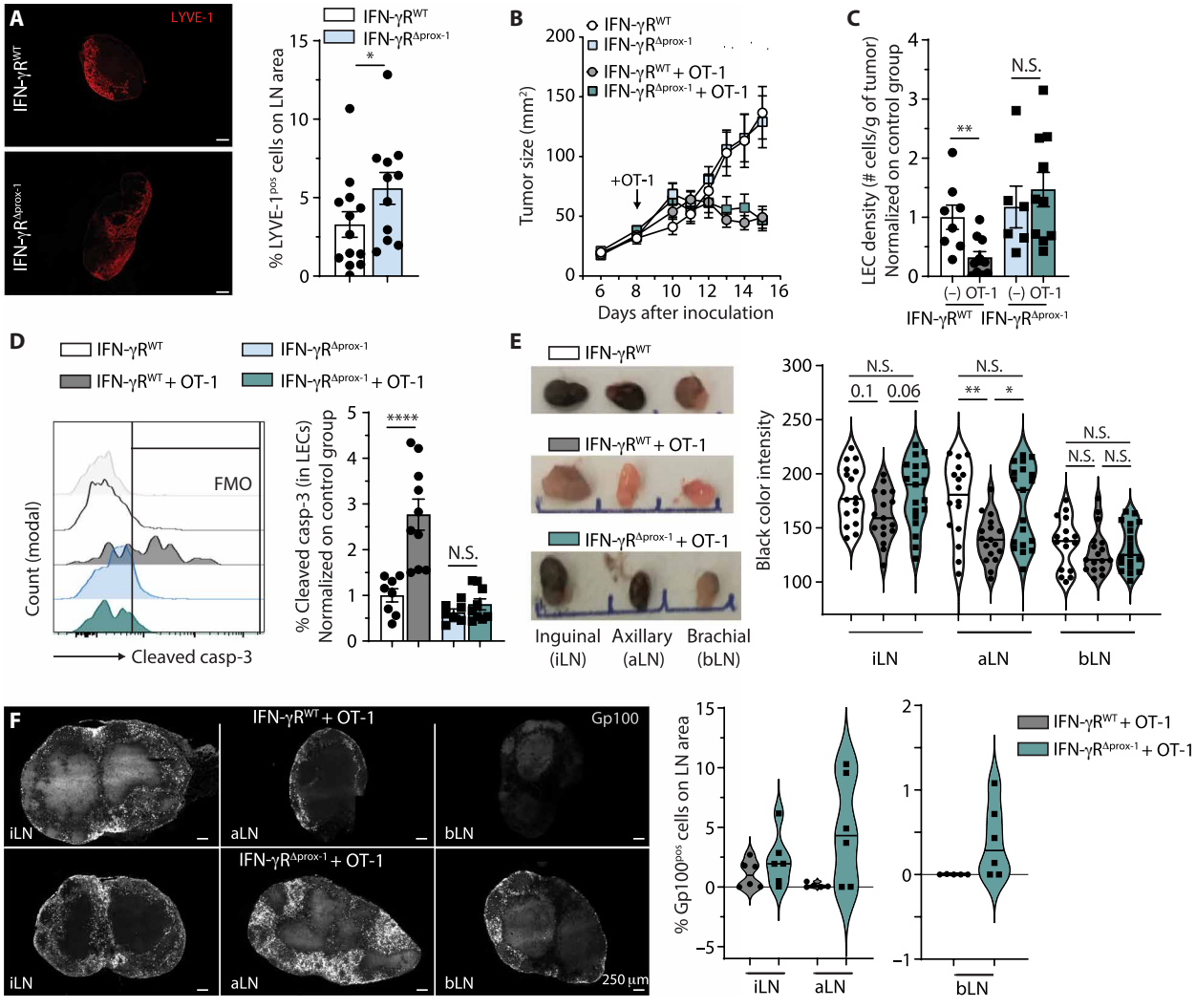

Fig. 4. IFN-γR signaling in LECs is indispensable to ATT-mediated tumor LV destruction. (**A**) Lyve-1 staining of ndLN (non dLN) sections from IFN-γR^{WT} and IFN-γR$^{\Delta prox\text{-}1}$ mice 4 weeks after tamoxifen treatment. (**B** to **F**) Tamoxifen-treated IFN-γR^{WT} and IFN-γR$^{\Delta prox\text{-}1}$ mice were injected or not with 0.5 × 10^6 in vitro activated OT-1 cells 8 days after B16F10-OVA^{+}VC^{+} inoculation. (B) Tumor growth. Data are representative of three experiments. (C) Tumor LEC density and (D) frequency of cleaved casp-3^{+} tumor LEC 5 days after T cell injection. Data represent two pooled experiments, $N = 6$ to 10 mice per group. (E) Black color intensity analysis of inguinal, axillary, and brachial TdLN from indicated mice 6 days after OT-1 transfer. Pictures show representative images, and histograms show the quantification of the intensity for individual LNs. Data are pooled from three experiments, $N = 16$ mice per group. (F) Gp100 staining of inguinal, axillary, and brachial TdLNs from indicated mice 9 days after OT-1 transfer. Pictures show representative images, and histograms show the quantification of Gp100^{+} cells in LNs. Data are from six mice per group. (A, C, and D) Mann-Whitney statistical test; (B) two-way ANOVA test; (E) one-way ANOVA test. Error bars show means ± SEM.*$P < 0.05$, **$P < 0.01$, ****$P < 0.0001$.

compared to IFN-γR^{WT} mice (Fig. 4A), tumor LVD and frequency of cleaved casp-3^{+} tumor LECs were not different between the two groups in the absence of OT-1 transfer (Fig. 4, C and D), suggesting that the IFN-γ produced by endogenous immune cells is not sufficient to induce B16F10-OVA^{+}VC^{+} tumor LEC apoptosis. Notably, OT-1 effector transfer also reduced tumor BEC density (fig. S6F) and induced BEC apoptosis (fig. S6G) in both IFN-γR^{WT} and IFN-γR$^{\Delta prox\text{-}1}$ mice.

We next investigated the impact of OT-1–induced LV dismantling, as well as the requirement of IFN-γ signaling, on metastasis establishment in TdLNs. In the absence of OT-1 transfer, TdLNs from B16F10-OVA^{+}VC^{+} tumor-bearing IFN-γR^{WT} and IFN-γR$^{\Delta prox\text{-}1}$ mice exhibited similar levels of metastasis (fig. S6H), ruling out the possibility that increased LVD observed at steady state in IFN-γR$^{\Delta prox\text{-}1}$ LNs (Fig. 4A) would provide a better metastatic niche compared to IFN-γR^{WT} LNs. The adoptive transfer of OT-1 in B16F10-OVA^{+}VC^{+} tumor-bearing IFN-γR^{WT} mice only modestly alters tumor metastasis in inguinal TdLNs, while it significantly reduced tumor metastasis in axillary TdLNs (Fig. 4E). In contrast, both inguinal and axillary TdLNs from adoptively transferred B16F10-OVA^{+}VC^{+} tumor-bearing IFN-γR$^{\Delta prox\text{-}1}$ mice showed more metastasis compared to control IFN-γR^{WT} mice (Fig. 4E). Tumor regression induced by OT-1 effector transfer was identical in IFN-γR$^{\Delta prox\text{-}1}$ and IFN-γR^{WT} mice (Fig. 4B), ruling out the possibility that differences in primary tumor size would account for the modulation of TdLN metastasis. Gp100 immunofluorescent staining demonstrated that, upon OT-1 transfer, metastatic foci were increased in TdLNs from B16F10-OVA^{+}VC^{+} tumor-bearing IFN-γR$^{\Delta prox\text{-}1}$ mice compared to IFN-γR^{WT} mice (Fig. 4F). After OT-1 transfer, the number of metastatic positive LNs was generally higher in B16F10-OVA^{+}VC^{+} tumor-bearing IFN-γR$^{\Delta prox\text{-}1}$ mice compared to IFN-γR^{WT} mice, with significant difference in black color intensity in inguinal and axillary TdLNs (fig. S6, I and J). In addition, OT-1 frequencies were found similar in TdLNs of IFN-γR^{prox1} and IFN-γR^{WT} mice (fig. S6K), dismissing a potential difference in the local control of metastasis by CTLs in LNs. Together, these data indicate that the reduction in tumor LV induced by tumor-specific effector CD8^{+} T cells inhibits metastasis in TdLNs in an IFN-γR–signaling dependent manner.

CTLs eliminate LECs through antigenic contact and killing

Manipulating CTL killing activity in tumors represents an attractive immunotherapeutic approach. CTLs kill target cells on the basis of antigenic peptide MHCI recognition through the release of cytotoxic molecules. IFN-γ enhances antigen processing and presentation in tumor cells, which, in turn, promotes their recognition and killing by T cells (*49*). Hence, promoting the production of IFN-γ by CTLs leads to enhanced antitumor responses in vivo in mouse models (*50*, *51*). In vitro, LEC killing by OT-1 cells was found to be dependent on the number of T cells transferred and required preloading of LECs with OVA peptide (Fig. 5A). Soluble IFN-γ favored, as expected, PD-L1 and MHCII expression on LECs (fig. S7, A and B), testifying LEC responsiveness to the cytokine. However, IFN-γ signaling was not sufficient to promote LEC apoptosis (Fig. 5A), suggesting that antigen-dependent CTL-LEC interactions are necessary. In vivo, multiple intratumoral injections of high doses (1.5 μg twice a day for 4 days) of IFN-γ significantly reduced tumor growth (fig. S7C), likely due to the proapoptotic function of the cytokine on tumor cells. However, although this treatment efficiently induced the up-regulation of IFN-γ–responsive genes PD-L1 and MHCII by tumor LECs (fig. S7, D and E), it did not induce cleaved casp-3 expression by tumor LECs (fig. S7F), confirming that IFN-γ is not sufficient to induce tumor LEC apoptosis. It has been previously published that IFN-γ negatively regulates LN LECs by inhibiting sprouting lymphangiogenesis and decreased markers of LEC fate, without, however, evidencing any direct effect on LEC apoptosis (*46*). Furthermore, LECs from steady-state skin and from B16F10-OVA^{+}VC^{+} tumors expressed significantly lower levels of IFN-γR compared to TdLN and non-dLN LECs (fig. S7G), suggesting that LECs from different organs may respond differently when exposed to similar cytokine milieu.

To firmly determine whether OT-1 selectively eliminates LECs presenting their cognate antigenic peptide, OT-1 effectors were incubated with WT (GFP^{+}) and β_2m^{KO} (β2-microglobulin) (GFP^{neg}) LEC cocultures, loaded or not with OVA peptide, and treated or not with IFN-γ blocking antibodies or granzyme-B inhibitor. Effector CD8^{+} T cells induced cleaved casp-3 expression exclusively in OVA peptide–loaded WT LECs (Fig. 5B), resulting in a lower proportion of WT LECs compared to β2m^{KO} LECs (fig. S7H). Those effects were abolished in the presence of granzyme-B inhibitor (Fig. 5B and fig. S7H). In contrast, IFN-γ blocking antibodies did not prevent LEC apoptosis, demonstrating that IFN-γ does not exert a direct proapoptotic effect (Fig. 5B and fig. S7H). Live imaging experiments also showed that OVA-loaded WT (GFP^{+}) LECs, but not OVA-loaded β_2m^{KO} (GFP^{neg}) LECs, expressed cleaved casp-3 and underwent apoptosis after establishing an antigenic synapse with OT-1 effector T cells (Fig. 5C and movie S1).

We next compared the ability of different doses of high–TCR affinity OT-1 and low–TCR affinity OT-3 effector T cells (*52*) to induce the expression of cleaved casp-3 in LECs in vitro. OT-3 cells were less efficient at inducing LEC apoptosis (fig. S7I). Therefore, in vitro LEC killing requires the establishment of cognate antigen-specific synapses with high-affinity TCR CTLs.

CTLs induce apoptosis in tumor-antigen cross-presenting tumor LECs, resulting in LN metastasis inhibition

We have shown that B16F10-OVA^{+}VC^{+} tumor LECs exhibit the ability to capture and process exogenous antigens (*35*). Furthermore, LECs are capable of antigen cross-presentation in steady-state LNs (*53*), TdLNs, and tumors (*31*). To determine whether, as demonstrated in vitro, the killing of tumor LECs is also dependent on antigen-specific cognate interaction with CTLs in vivo, we first assessed the ability of tumor LECs to function as antigen cross-presenting cells. LECs (CD45^{-}CD31^{+}gp38^{+}) and DCs (CD45^{+}CD11c^{hi}MHCII^{+}) were isolated from B16F10-OVA^{+}VC^{+} tumors, and mRNA levels of genes implicated in the MHCI-restricted antigen (cross-)presentation pathways were evaluated. *H-2K^{b}*, *B2m*, *Nlrc5*, *Tap-1*, and *Lmp2* mRNAs were significantly induced in tumor LECs from IFN-γR^{WT} control mice 4 days after the transfer of OT-1 effectors (Fig. 6A). In notable contrast, tumor LECs from IFN-γR$^{\Delta prox\text{-}1}$ mice expressed lower mRNA levels of all these genes with or without OT-1 transfer (Fig. 6A), demonstrating that IFN-γ signaling in tumor LECs promotes their ability to function as bona fide antigen (cross-)presenting cells. The fold induction of the different mRNAs after OT-1 transfer was superior in tumor LECs from IFN-γR^{WT} mice compared to tumor DCs, which otherwise behaved similarly in IFN-γR^{WT} and IFN-γR$^{\Delta prox\text{-}1}$ mice (fig. S8).

On the basis of the observation that cancer cell apoptosis was induced in B16F10-OVA^{+}VC^{+} tumors following OT-1 effector

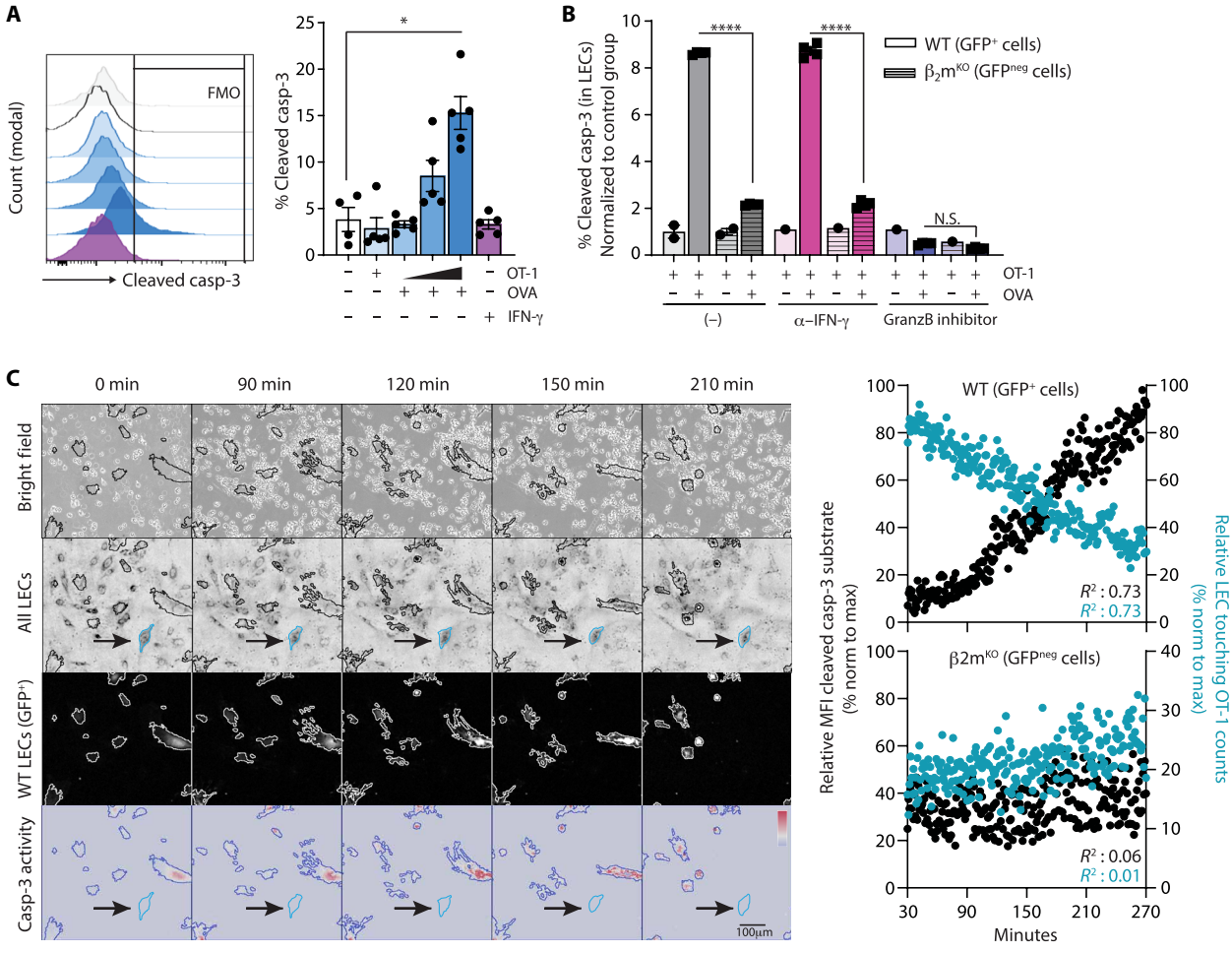

Fig. 5. CTLs induce LEC apoptosis through antigen-specific interactions. (**A**) LEC/FRC cultures were loaded or not with OVA peptide (OVA) and incubated with either different ratios of in vitro activated OT-1 cells (1:10, 1:3, and 3:1 OT1:LEC/FRC) or soluble IFN-γ. Frequencies of cleaved casp-3$^+$ LECs after 14 hours. Data are representative of two independent experiments. Each point represents a technical replicate. (**B**) WT (LC3-GFP$^+$) or β_2m^{KO} (GFP^{neg}) LEC/FRC cultures were loaded or not with OVA and incubated or not with anti–IFN-γ antibodies and granzyme-B inhibitor. In vitro activated OT-1 cells were added in the cultures and frequencies of cleaved casp-3$^+$ WT and β_2m^{KO} LECs (gated on CD45^{neg}CD31$^+$gp38$^+$ cells) 14 hours later. Data are from one experiment. (**C**) Sorted WT (LC3-GFP$^+$) and β_2m^{KO} (GFP^{neg}) LEC cocultures (ratio of 1:1) were loaded with OVA and in vitro activated OT-1 cells were added (OT-1:LEC ratio of 10:1), and time-lapse imaging was performed (see movie S1). Representative images at indicated time points of bright field, all LECs, WT LC3-GFP$^+$ LECs, and cleaved casp-3 activity. The arrows indicate one example of β_2m^{KO} (GFP^{neg}) LECs. Graphs represent the relative MFI of cleaved casp-3 substrate (left *y* axis) and the relative frequency of OT-1 touching LECs (right *y* axis) in WT and β_2m^{KO} LECs. Data are representative pooled from three experiments. (A) Mann-Whitney statistical test. Error bars show means ± SEM. (C) Linear regression. *P < 0.05, ****P < 0.0001.

transfer (fig. SA), we hypothesized that, upon ATT, tumor LECs exposed to IFN-γ would acquire the ability to cross-present tumor antigens released by CTL-mediated tumor destruction. Therefore, we measured the expression levels of MHCI-OVA complexes at the surface of LECs in B16F10-OVA$^+$VC$^+$ tumors from mice adoptively transferred with 0.05×10^6 or 0.5×10^6 OT-1 effectors. MHCI-OVA complexes were up-regulated by tumor LECs in a T cell dose-dependent manner, and more at day 5 compared to day 3 after ATT (Fig. 6B). In line with our hypothesis, we found that tumor LECs underwent apoptosis upon antigen-specific interaction with CTLs and that cleaved casp-3 was specifically up-regulated by MHCI-OVA$^+$ tumor LECs (Fig. 6C).

Supporting the notion that effector T cells promote the ability of tumor LECs to cross-present tumor antigens, OVA + CpG-B vaccination of B16F10-OVA$^+$VC$^+$ tumor-bearing mice resulted in an increased expression of MHCI-OVA complexes by tumor LECs (fig. S9B). Similarly, LECs from MC38-OVA$^+$VC$^+$ tumors, which contained elevated CTL numbers (fig. S4F), expressed increased levels of MHCI-OVA complexes compared to LECs from B16F10-OVA$^+$VC$^+$ tumors (fig. S9C). In addition, B16F10-OVA$^+$VC$^+$ tumor LECs expressed increased levels of MHCI-OVA complexes following the adoptive transfer of Pmel-1 effectors or after vaccination with Gp100 + CpG (fig. S8D), demonstrating that tumor cell killing by CTLs induces tumor antigen spreading for cross-presenting LECs.

The up-regulation of MHCI-OVA complexes by LECs derived from B16F10-OVA$^+$VC$^+$ tumors of IFN-γR^{WT} control mice was higher at day 8 compared to day 5 after injection of 0.5×10^6 OT-1 effectors and decreased again at day 16, likely due to variations of CTL-dependent tumor destruction followed by the release of tumor antigens over time (Fig. 6D). In contrast, the expression of MHCI-OVA complexes was almost fully abrogated in tumor LECs from

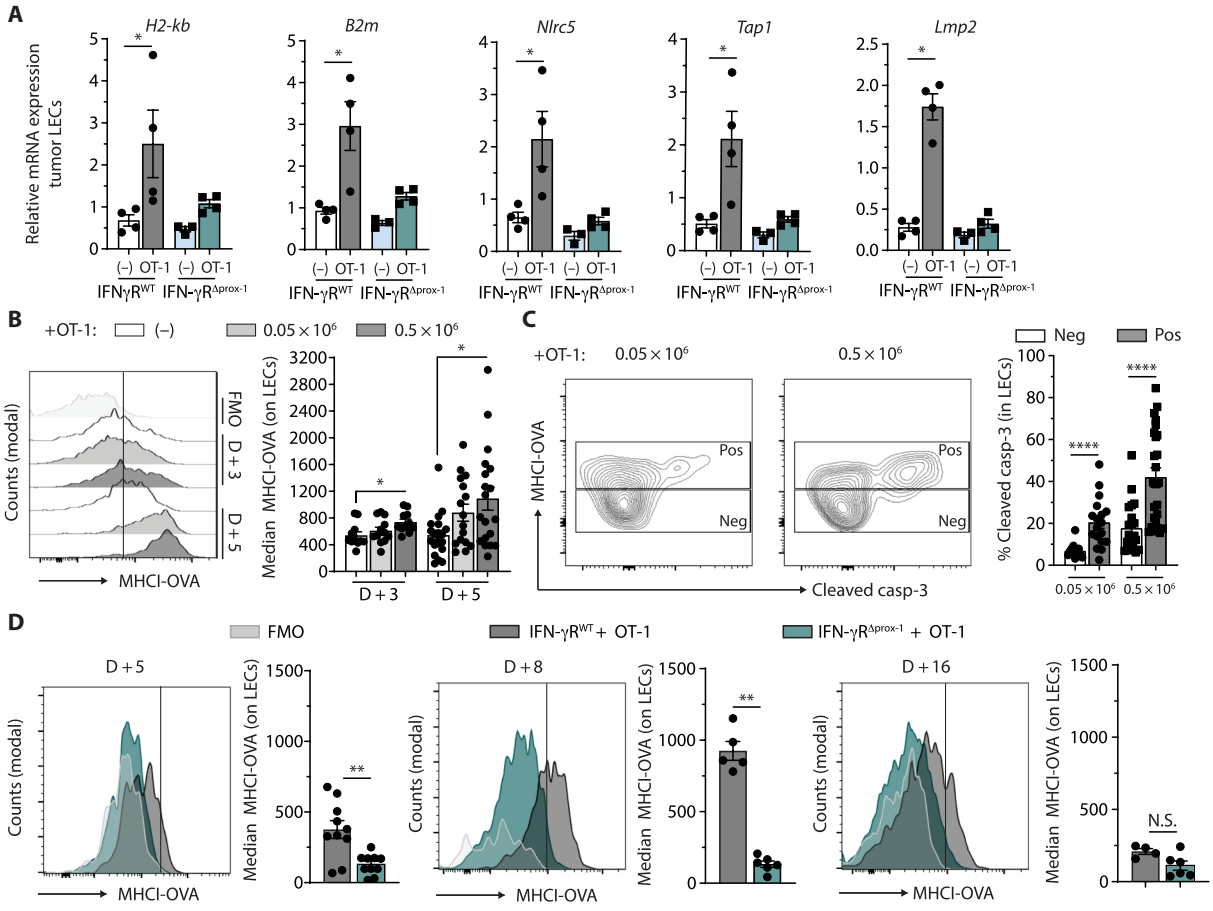

Fig. 6. CTLs induce the apoptosis of tumor-antigen cross-presenting tumor LECs in an IFN-γ–dependent manner. (**A**) Tamoxifen-treated IFN-γR^{WT} and IFN-γR$^{\Delta prox\text{-}1}$ mice were injected or not with 0.5 × 10^6 OT-1 cells 9 days after B16F10-OVA$^+$VC$^+$ inoculation. mRNA levels of indicated genes in tumor LECs 4 days later. Data are from one experiment, $N = 3$ to 4 mice per group. (**B** and **C**) C57BL/6 mice were injected or not with 0.05 × 10^6 or 0.5 × 10^6 OT-1 cells 9 days after B16F10-OVA$^+$VC$^+$ inoculation. (B) MHCI-OVA complex levels in tumor LECs at days 3 and 5 after OT-1 transfer. (C) Frequencies of cleaved casp-3 among MHCI-OVA^{neg} (Neg) and MHCI-OVA^{pos} (Pos) LECs 5 days after transfer. (**D**) Tamoxifen-treated IFN-γR^{WT} and IFN-γR$^{\Delta prox\text{-}1}$ mice were injected with 0.5 × 10^6 OT-1 cells 9 days after B16F10-OVA$^+$VC$^+$ inoculation. MHCI-OVA complex levels in tumor LECs at days 5, 8, and 16 after OT-1 transfer. Data are from one experiment, $N = 4$ to 10 mice per group. (A, C, and D) Mann-Whitney statistical test; (B) one-way ANOVA test. Error bars show means ± SEM. *$P < 0.05$, **$P < 0.01$, ****$P < 0.0001$.

IFN-γR$^{\Delta prox\text{-}1}$ mice (Fig. 6D), establishing a direct link between IFN-γ signaling and antigen cross-presentation in tumor LECs.

To prove that MHCI-restricted tumor antigen presentation is a prerequisite for LEC killing by CTLs, we adoptively transferred OT-1 effectors in B16F10-OVA$^+$VC$^+$ tumor-bearing WT and β_2m^{KO} mice, which lack MHCI expression. In the absence of OT-1, LVD was similar between WT and β_2m^{KO} mice (fig. S10A). OT-1 transfer similarly reduced tumor growth in C57BL/6 and β_2m^{KO} mice (Fig. 7A), and the density of IFN-γ$^+$ and granzyme-B$^+$ OT1 was identical in both groups (fig. S10B). PD-L1 and MHCII molecules were also up-regulated in a similar fashion by tumor LECs in both groups (fig. S10, C and D). In contrast, tumor LECs from β_2m^{KO} mice did not express MHCI-OVA complexes (fig. S10E). The induction of cleaved casp-3 in tumor LECs by OT-1 transfer observed in WT mice was completely abolished in LECs from β_2m^{KO} mice (Fig. 7B), demonstrating that MHCI expression by LECs is crucial for LV killing by OT1 cells. Last, we have generated mice in which the absence of β_2-microglobulin (β_2m) is restricted to LECs by crossing Prox-1Cre^{ERT2} mice with β_2m$^{flox/flox}$ mice (β_2m$^{\Delta prox\text{-}1}$). B16F10-OVA$^+$VC$^+$ tumor-bearing control β_2m^{WT} and β_2m$^{\Delta prox\text{-}1}$ mice were adoptively transferred with OT-1 effectors. Tumor growths were similar in both groups (Fig. 7C), as well as the density of OT-1 effector infiltrating the tumors (fig. S10F). While PD-L1 and MHCII expression by LECs were identical in tumors isolated from β_2m^{WT} and β_2m$^{\Delta prox\text{-}1}$ mice (fig. S10, G and H), LECs from β_2m$^{\Delta prox\text{-}1}$ tumors do not express MHCI-OVA (fig. S10I). Tumor LEC apoptosis was reduced (Fig. 7D) in β_2m$^{\Delta prox\text{-}1}$ mice compared to β_2m^{WT} mice, firmly demonstrating that MHCI expression by LEC is required for their killing by CTLs. Last, both the number of metastasis-positive LNs (Fig. 7E) and the number of metastatic foci per LNs (Fig. 7F) were augmented in β_2m$^{\Delta prox\text{-}1}$ mice compared to β_2m^{WT} mice adoptively transferred with OT-1 effectors (Fig. 7F). These experiments firmly demonstrate that MHCI expression by LEC is required for their killing by CTLs, leading to the control of LN metastasis.

DISCUSSION

Immunotherapy has been the hallmark progress in the treatment of cancer over the last decade. Multiple immunotherapeutic approaches aiming at improving T cell responses, such as immune checkpoint

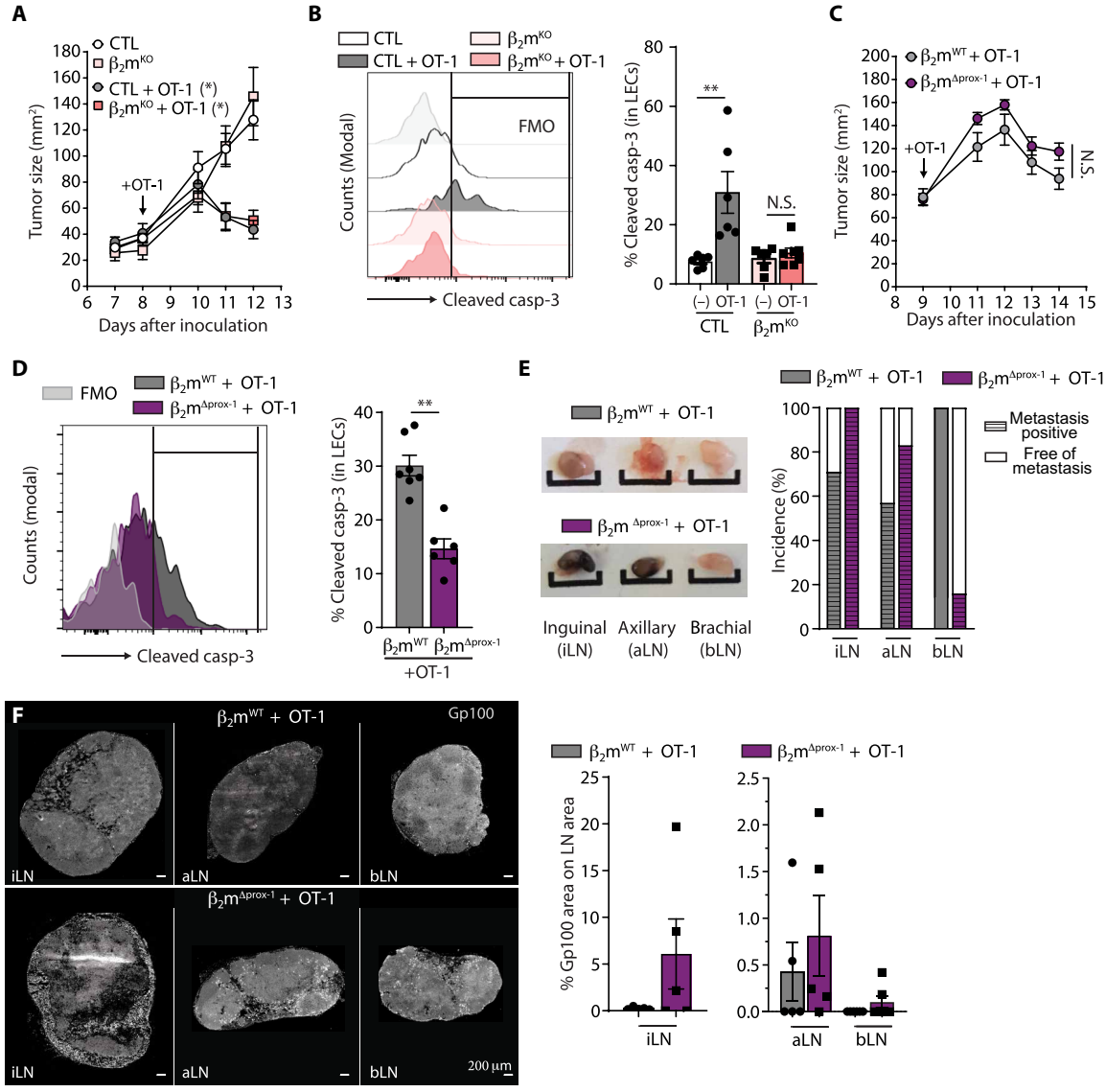

Fig. 7. T cell–mediated LEC apoptosis requires MHCI expression on tumor LECs. (**A** and **B**) C57BL/6 and β_2m^{KO} were injected or not with 0.5×10^6 OT-1 cells 8 days after B16F10-OVA$^+$VC$^+$ inoculation. (A) Tumor growth and (B) frequencies of cleaved casp-3$^+$ tumor LECs 4 days after OT-1 transfer. Data are from one experiment, $N = 6$ to 7 mice per group. (**C** to **F**) Tamoxifen-treated β_2m^{WT} and $\beta_2m^{\Delta prox\text{-}1}$ mice were injected with 0.5×10^6 OT-1 cells 9 days after B16F10-OVA$^+$VC$^+$ inoculation. (C) Tumor growth and (D) frequencies of cleaved casp-3$^+$ tumor LECs 5 days after OT-1 transfer. Data are from one experiment, $N = 6$ to 7 mice per group. (E) The percentage of metastasis-positive and metastasis-negative (free of metastasis) LNs according to black color. Pictures show representative images. Scale bars, 0.5 cm. (F) Immunofluorescent Gp100 staining of inguinal, axillary, and brachial TdLNs (iLN, aLN, and bLN, respectively) 5 days after OT-1 transfer. Histograms represent the quantification of Gp100$^+$ cells in LNs. (A and C) Two-way ANOVA test; (B, D, and E) Mann-Whitney statistical test. Error bars show means ± SEM. *$P < 0.05$, **$P < 0.01$.

blockade, adoptive cellular therapies, and cancer vaccines, represent powerful tools in the fight against cancer. Although tumor-associated lymphangiogenesis has been shown to increase the responsiveness of the TME to immunotherapies (*28*), it simultaneously dampens the efficacy of antitumor cytotoxic T cell responses by enhancing immunosuppression (*31*, *34*, *35*, *54*). In this study, we focused our research on LV alteration by therapies involving antitumor effector CD8$^+$ T cell responses. As previously shown, we observed that the immunosuppressive phenotype of tumor LECs is stronger in immunogenic tumors (MC38-OVA-VC$^+$) compared to less-immunogenic ones (B16-OVA-VC$^+$) or following adoptive T cell and vaccination strategies, therefore altering the efficacy of those approaches. However, when the scales are tipped toward potent T cell responses, boosting of antitumor cytotoxic T cell density not only promotes cancer cell death and tumor rejection but also triggers tumor LEC apoptosis and LV dismantling. Increasing effector CD8$^+$ T cells in tumors enhances the expression of the proapoptotic marker cleaved casp-3 in tumor LECs, leading to reduced LV densities. The decrease in LVs was found more pronounced at the center of the tumor compared to the periphery of the tumor, which is reminiscent with the observation that T cells attack the tumor vasculature predominantly inside the tumor mass (*55*). CTL transfer also resulted in BEC

apoptosis and reduced densities in tumors, suggesting a broader mechanism of nonhematopoietic, or at least endothelial, cell death in the presence of potent cytotoxic T cell responses.

Using different tumor models and different T cell–based immunotherapeutic approaches, we show that enhanced infiltration of tumor-specific T effector positively correlated to the frequency of apoptotic tumor LECs. These results suggest that a certain threshold of CTL density in tumors is necessary to overcome IFN-γ–mediated LV immunosuppression by inducing tumor LEC apoptosis and concomitant LV destruction.

Cytotoxic T cells can kill target cells bearing specific cognate peptide-MHCI complexes via direct cell-cell contact, while ignoring healthy bystander cells lacking cognate peptide-MHCI complexes. As previously observed, after being adoptively transferred, OVA-specific $CD8^+$ effector OT-1 cells infiltrate the stroma of OVA-expressing lymphangiogenic melanoma, localize, and cluster in close proximity to tumor LV (*31*). LECs were demonstrated to capture, process, and cross-present exogenous antigen, leading to $CD8^+$ T cell clustering and suppression at steady state (*31*, *53*, *56*, *57*) and in a tumor context (*31*). We show that molecules implicated in MHCI-restricted (cross-)presentation pathways (such as NLRC5 (NLR Family CARD Domain Containing 5), TAP1 (Transporter associated with antigen processing 1), LMP2 (Latent Membrane Protein 2), MHCI, and β_2m) are up-regulated by tumor LECs in mice that have received ATT. The expression level of these genes is higher in tumor LECs compared to total tumor $CD11c^{hi}MHCII^+$ DCs. However, it is possible that specific DC subsets, or DCs in TdLNs, exhibit an increased ability to cross-present tumor antigens. LECs in OVA-expressing melanomas and their TdLNs express MHCI-SIINFEKL peptide (MHCI-OVA) complexes at their surface (*31*), suggesting that LECs in tumors can function as antigen cross-presenting cells. An alternative possibility is that preprocessed antigenic peptides released in the TME directly bind MHCI molecules expressed at the surface of tumor LECs.

Furthermore, we show that B16-OVA-VC^+ tumor LECs up-regulate MHCI-OVA complexes when treated with ATT or vaccination, suggesting that antigen-specific interactions with effector T cells induce apoptosis in tumor LECs. Accordingly, cleaved casp-3 expression is specifically enhanced in tumor LECs expressing MHCI-OVA complexes. In B16F10-OVA^+ tumors that do not overexpress VEGF-C and contain very low LEC numbers, frequencies of cleaved casp-3 LECs were notably elevated compared to B16F10-OVA^+VC^+ tumors already in the absence of ATT, suggesting that elevated CTL/LEC ratio might enhance tumor LEC killing by infiltrating CTLs. VEGF-C has been described to exhibit cytoprotective effects on LECs (*58*). Therefore, it is likely that, in addition to direct killing by CTL, elevated amounts of VEGF-C in B16F10-OVA^+VC^+ tumors compared to B16F10-OVA^+ tumors protect tumor LEC from apoptosis. Together, our data support the hypothesis that LEC apoptosis induced by CTLs is T cell dose dependent and TCR affinity/avidity dependent.

Our in vitro and in vivo experiments demonstrate that LEC apoptosis induced by CTLs is abolished when LECs are deficient for β_2m molecules, demonstrating that ATT eliminates LECs through TCR-MHCI/tumor antigen interactions. It has been shown that the presentation of high-affinity ligands (peptide MHCI complexes) by cancer cells and/or the tumor stroma is required for cytokine production by T cell, stroma destruction, and relapse-free tumor regression (*59*). We provide evidence that the efficacy of LEC killing by CTLs relies on direct TCR recognition most likely via high-affinity and/or high-avidity interactions. LEC apoptosis induced by CTLs is T cell dose dependent, indicating that the ratio between LECs and T cells is a critical parameter. In vivo, the transfer of effector Pmel-1 T cells, which express a TCR recognizing the low-affinity peptide Gp100 (*59*), is inefficient at inducing tumor LEC death and LV destruction and requires concomitant vaccination with Gp100 + CpG-B. Accordingly, OVA-specific low–TCR affinity OT-3 effector T cells are less efficient to promote LEC apoptosis compared to high–TCR affinity OT-1 T cells in vitro. Those findings imply that the selection of T cells with high TCR affinity for tumor-specific peptide-MHCI complexes for immunotherapies will not only promote the killing of cancer cells but also induce tumor LEC death. In addition, peptide-derived vaccine strategies aiming at enhancing T cell priming by DCs could also enhance peptide loading and presentation by tumor LECs and may help to disrupt the tumor-associated LV.

Our results indicate that tumor antigen release promotes the cross-presentation of tumor antigens by LECs, allowing their subsequent antigen-dependent killing by CTLs. Consistent with the hypothesis that CTL killing of tumor cells would increase the availability of tumor antigens for cross-presentation by LECs, we show that Pmel-1 effector transfer in B16F10-OVA^+VC^+ tumor-bearing mice enhances the expression of MHCI-OVA complexes by tumor LECs. This indicates that tumor antigen spreading for cross-presenting LECs occurs in the context of immunotherapy and will likely enlarge the breadth of $CD8^+$ TCR repertoires and will amplify antigen-specific LEC killing by CTLs.

IFN-γ has been shown to play a dual and opposite role in cancer development. IFN-γ signaling not only enhances PD-L1 expression on tumor cells, inhibiting antitumor immunity (*60*), but also augments antigen processing and presentation, which, in turn, enhances their recognition and cytolysis by T cells (*61*). In developing tumors, the expression of PD-L1 and MHCII molecules by tumor LECs are dependent on IFN-γR signaling. We show that IFN-γ produced intratumorally during ATT further enhances the expression of PD-L1 and MHCII by tumor LECs, which will likely promote their immunosuppressive functions (*34*, *35*, *61*). Following ATT, IFN-γ in LECs further increases their expression of the MHCI transactivator NLRC5- and MHCI-related genes, stimulating the antigen processing and presentation machinery in LECs, as was also shown for tumor cells (*62*). This mechanism could be useful to potentiate LEC killing by tumor-specific CTL through an antigen-dependent pathway. By using conditional KO mice in which LECs do not express IFN-γR, we observed that both the inhibition of tumor LVD and the induction of LEC apoptosis induced by ATT are abolished in the absence of IFN-γR signaling in LECs, demonstrating that IFN-γ is crucial for their killing by CTLs. CTLs destroy their target cells through different pathways, triggering programmed intracellular events in target cells and leading to apoptotic cell death: the granule exocytosis (perforin/granzymes), the secretion of proinflammatory molecules (IFN-γ/TNF), and the expression of cell death ligand [FasL/ TRAIL (tumor-necrosis-factor related apoptosis inducing ligand)] (*63*). In vitro, we observed that LEC killing by CTLs is abrogated by the addition of granzyme-B inhibitor, suggesting that involvement of this pathway in CTLs induced tumor LEC apoptosis. The addition of elevated doses of IFN-γ alone does not favor the expression of cleaved casp-3 in LECs, confirming that LEC death is not a direct consequence of a proapoptotic effect of IFN-γ. Further investigations need to be performed to validate the implication of the granzyme pathway

in vivo. Together, our data show that LEC killing by CTLs is dependent on IFN-γR signaling in LECs, which promotes their ability to cross-present tumor-derived antigenic peptides and to become CTL targets. However, we cannot rule out the possibility that IFN-γ further contributes to the pathway by directly modulating the expression of molecules implicated in tumor cell adhesion and transmigration through the lymphatic endothelium.

Tumor lymphangiogenesis and the remodeling of LVs are important steps in tumor cell dissemination. Cancer metastasis propagates through LVs to first reach the sentinel LNs and further colonize distant organs (*3*, *4*). Our data show that T cells in tumors not only can support immunosuppressive functions of tumor LECs but also can induce their apoptosis. Which of the two opposite effects dominate depends on the number and affinity of CTLs attacking the tumor. Tumor LEC apoptosis and LV destruction by CTLs resulted in altered lymphatic drainage to TdLNs and reduced LN metastasis. Although we cannot firmly rule out a direct effect of CTL transfer on LN metastasis or the preexistence of undetectable micrometastasis in LNs at the time of CTL transfer, the reduced transport of injected tumor cells to TdLNs suggests that tumor LV disruption prevents tumor cell migration from primary tumors and subsequent transit to LNs. This is further supported by the fact that, upon OT-1 CTL adoptive transfer, TdLN metastasis are significantly increased in IFN-γR^{prox1} compared to IFN-γR^{WT} mice, and this is despite similar OT-1 CTL frequencies in TdLNs. It has been shown that lymphangiogenesis in TdLNs is part of the formation of the LN premetastatic niche and is associated with metastasis formation (*10*, *17*, *18*). However, metastatic scores in LNs from tumor-bearing conditional KO mice in which LECs do not express IFN-γR were not affected in the absence of CTL transfer, indicating that the disruption of tumor-associated LVs, and not alterations of LN premetastatic niches, is responsible for reduced LN metastasis after ATT. Last, we observed a significant reduction of LN metastasis in both primary (inguinal) and secondary (axillary and brachial) TdLNs. Further investigation will determine whether decreased metastasis in secondary TdLNs results from reduced inguinal LN burden or from a failure to sequentially colonize downstream LNs.

ATT and vaccination aiming at enhancing antitumor CTL responses and tumor cell killing represent up-and-coming strategies to fight cancers. Because LVs represent the main route for tumor cell spreading and dissemination to sentinel LNs and concomitant spreading to distal organs, our data reveal an unexpected mechanism by which tumor-associated LVs can be modulated by CTLs and metastasis can be reduced. Deciphering the mechanisms in LV destruction by antitumor CTLs, as well as determining the numbers of CTLs required to induce efficient LV destruction, is important to pave the way for the development of new therapeutic strategies to inhibit tumor dissemination.

METHODS

Mice

C57BL/6N (B6) mice were purchased from Charles River Laboratories, France. Mice with a disrupted β_2M gene (hereafter called β_2M^{KO}) (*64*) were backcrossed onto the B6 background for at least 10 generations (from SwImMR, University of Zurich). To generate mice selectively lacking IFN-γR or β_2m in LECs (IFN-γR$^{\Delta prox\text{-}1}$ or $\beta_2m^{\Delta prox\text{-}1}$), IFN-γR2$^{fl/fl}$ (IFN-γR^{WT}) mice (*48*) or $\beta_2m^{fl/fl}$ (β_2m^{WT}) mice [purchased from Charles River Laboratories; B6(Cg)-B2mtm1c(EUCOMM)Hmgu/J, strain #: 034858, RRID:IMSR_JAX:034858] were crossed with Prox1-Cre^{ERT2} mice (*47*). $OVA_{257–264}$-specific TCR transgenic OT-1 CD45.1 mice (purchased from Charles River Laboratories), $OVA_{257–264}$-specific TCR transgenic OT-3 CD45.1 mice (*65*), and $Gp100_{25–33}$-specific TCR transgenic Pmel-1 mice (*66*), as well as LC3-GFP mice (*67*), were bred in our animal facility. All mice (male and female) were used between the ages of 6 and 12 weeks and bred and maintained under specific-pathogen–free conditions at the animal facility of Geneva Medical School and under SPF (specific-pathogen-free) conditions at Charles River Laboratories, France. All procedures were approved and performed in accordance to the guidelines of the animal research committee of Geneva under the license number GE79/20.

Tamoxifen treatment

Prox-Cre^{ERT2} IFN-γR2$^{fl/fl}$ (IFN-γR$^{\Delta prox\text{-}1}$) mice and IFN-γR2$^{fl/fl}$ (IFN-γR^{WT}) littermate control mice were treated intraperitoneally by injection with tamoxifen (T5648, Sigma-Aldrich), 1 mg per mouse twice a day for 4 days. Mice were used for experiments 2 weeks after the last injection.

Tumor cell lines

Mouse B16-F10 melanoma cells (American Type Culture Collection) were transfected with OVA (a gift from B. Huard) (B16F10-OVA$^+$), and B16F10-OVA$^+$ and B16F10 were engineered to overexpress VEGF-C (B16F10-OVA$^+$VEGF-C^{hi} or B16-VEGF-C^{hi}) as previously published (*31*) and were maintained in RPMI supplemented with 10% heat-inactivated fetal bovine serum (FBS), 100 μM penicillin-streptomycin, and 50 mM of β-mercaptoethanol. Geneticin was added after 1 day of culture to select OVA-expressing cells.

To obtain mouse MC38-VEGF-C^{hi} cells, MC38 cells (a gift from W. Reith) were transduced with a third-generation lentivirus encoding full-length mouse vegfc (NM_009506.2) under the control of EF1A promoter (VectorBuilder) and selected using puromycin (4 μg/ml). To generate retroviral m(mouse)OVA vector particles, the MigR1-OVA-IRES-GFP retroviral vector was cotransfected with the package plasmids pMD-gag/pol and pMD-VSV-G (all plasmids gifted by P. Romero) into human embryonic kidney 293T cells. The medium was changed with fresh full medium after 8 hours. Forty-eight hours later, the supernatants were harvested and filtered with a 0.45-μm filter and stored at −80°C (with the help of E. Cosset). MC38-VEGF-C^{hi} cells were transfected with supernatants containing OVA-GFP retrovirus, and MC38-OVA$^+$VEGF-C^{hi} cells were sorted by flow cytometry on the basis of GFP expression. Cells were maintained in Dulbecco's modified Eagle's medium (Gibco), 10% heat-inactivated fetal calf serum, 100 μM penicillin-streptomycin, and 50 mM β-mercaptoethanol.

Cell lines were not authenticated, used at below passage 20, and tested negative for *Mycoplasma*. Mouse VEGF-C protein levels from B16F10-OVA$^+$VEGF-C^{hi} and MC38-OVA$^+$VEGF-C^{hi} tumors were measured by using a mouse VEGF-C enzyme-linked immunosorbent assay kit (Cusabio), according to the manufacturer's instructions.

Tumor cell inoculation and tumor measurement

Mice were anesthetized using isoflurane or a mix of 2% Rompun (Bayer)/10% ketamine (Vetoquinol), and their backs were shaved. A total of 0.5×10^6 B16F10-OVA$^+$VEGF-C^{hi} cells, MC38-OVA$^+$VEGF-C^{hi} cells, or a mixture of B16F10-VEGF-C^{hi} and B16F10-OVA$^+$-VEGF-C^{hi} cells (ratio 9:1) were injected in 100 μl of phosphate-buffered saline

(PBS) subcutaneously on the back dorsolateral side. Primary tumor inoculation was controlled by measuring the distance between the front leg, the back leg, and the vertebral column of the mice, and the injection was always performed at the same distances from these three locations, at equal distance from the vertebral column and the back leg, representing approximately one-third of the distance to the front leg. Tumor size was monitored blindly every 1 to 2 days using a caliper, and tumor size was calculated by length × width. Mouse exclusion criteria are the following: tumor necrosis, tumor size >15 mm (diameter), and/or signs of pain or anxiety.

Tissue processing for flow cytometry and in vitro culture

LN cell isolation

For experiments involving the detection of fluorescent bead uptake by DCs or the presence of OT-1 in the TdLNs, LNs were cut into small pieces with scissors and digested in RPMI containing collagenase D (1 mg/ml; Roche) and deoxyribonuclease I (DNase I) (10 μg/ml; Roche) for 40 min at 37°C. After 20 min, solutions were mixed up and down and incubated for an additional 20 min at 37°C and filtered through a 70-μm cell strainer in fluorescence-activated cell sorting (FACS) buffer [PBS, 10% bovine serum albumin (BSA), and 5 mM EDTA], and single-cell suspensions were incubated with anti-CD16/CD32 antibody.

Stromal cell isolation

Tumors were cut into small pieces and digested in RPMI containing collagenase IV (1 mg/ml; Worthington Biochemical Corporation), DNase I (40 μg/ml; Roche), and 1% FBS for 30 min at 37°C. Samples were mixed up and down every 10 min. Tubes were centrifuged for a few seconds at 1500 rpm and supernatants were filtered through a 70-μm cell strainer in FACS buffer to stop the reaction. The remaining tissue was further digested in RPMI with collagenase D (1 mg/ml; Roche), DNase I (40 μg/ml; Roche), and 1% of FBS for 20 min at 37°C, with additional two cycles of repeated pipetting. The solution was filtered through a 70-μm cell strainer in FACS buffer and pooled into the first collected tubes.

OT-1, OT-3, Pmel-1, and polyclonal cell preparation

Spleens and LNs were smashed, filtered through a 70-μm mesh filter, and centrifuged at 1500 rpm for 5 min. Red blood cells were lysed with 1 ml of ammonium-chloride-potassium lysis buffer per spleen for 1 min. Following the addition of cell culture medium, splenocytes were washed and resuspended in complete medium (RPMI supplemented with 10% FBS, 1% penicillin-streptomycin, and 50 mM 2-β-mercaptoethanol).

LEC and fibroblastic reticular cell in vitro culture

A mixed LEC–fibroblastic reticular cell (FRC) culture was performed as previously described (*68*). Briefly, LNs from 6- to 8-week-old female mice (C57BL6N, LC3-GFP, or β_2m^{KO}) were dissected and digested with a freshly prepared enzymatic solution containing RPMI 1640 (Gibco), dispase (0.8 mg/ml) (Gibco), collagenase P (0.2 mg/ml) (Roche), and DNase I (0.1 mg/ml) (Roche). Tubes containing the digestion mixture were incubated at 37°C in a water bath, and every 10 min, LNs were gently mixed using a 1-ml pipette and, thereafter, the supernatant was filtered through a 70-μm cell strainer on 10 ml of cold FACS buffer containing 0.5% BSA (AppliChem) and 5 mM EDTA (AppliChem) in PBS. These steps were repeated every 10 min until all LNs were completely digested. Cells were washed and filtered through a 70-μm cell strainer, quantified using a hemocytometer, and plated in a T75 flask [coated with human fibronectin (10 μg/ml) (Millipore) and PureCol (10 μg/ml) (Advanced BioMatrix) for 30 min at 37°C] at a concentration of 4×10^7 to 6×10^7 cells per well. The LEC-FRC cell culture medium was minimum essential medium–α (Gibco) supplemented with heat-inactivated, 10% batch-tested, low immunoglobulin FBS (Gibco) and 1% penicillin/streptomycin (Gibco). Plates were washed and the culture medium was renewed every day to remove nonadherent cells. After 6 to 7 days, cultures primarily contained LECs and FRCs. Cells were detached with Accutase (Thermo Fisher Scientific) for 5 min at 37°C and plated on a 24-well plate (precoated with fibronectin and PureCol) at a concentration of 0.1×10^6 to 0.2×10^6 cells per well. In some experiments, cells were treated with IFN-γ (PeproTech; 10 μg/ml) for 14 hours.

Vaccination

OVA + CpG-B vaccination

B16F10-OVA$^+$VEGF-C^{hi} tumor-bearing mice were injected subcutaneously at day 5 with OVA protein (50 μg per mouse; Invivogen) and CpG-B 1668 (30 μg per mouse; Invivogen).

Gp100 + CpG-B vaccination

B16F10-OVA$^+$VEGF-C^{hi} tumor-bearing mice were injected subcutaneously at day 5 with human Gp100 peptide (KVPRNQDWL) (100 μg per mouse; Thermo Fisher Scientific) and CpG-B 1668 (30 μg per mouse; Invivogen).

Irradiated B16F10 VC$^+$ + CpG-B vaccination

B16F10 VC$^+$ tumor-bearing mice were injected subcutaneously at day 8 with irradiated B16F10-VC$^+$ [100 gray (Gy)] and CpG-B 1668 (30 μg per mouse; Invivogen).

CTL activation, adoptive transfer, and coculture with LEC-FRC

Splenocytes and LNs from 6- to 8-week-old OT-1, OT-3, Pmel-1, and C57BL/6N female mice were prepared as mentioned above (see the "Tissue processing for flow cytometry and in vitro culture" section). OT-1 and OT-3 cells were stimulated with 1 nM of OVA peptide (SIINFEKL) (Sigma-Aldrich) in the presence of interleukin-2 (IL-2) (100 U/ml) (PeproTech) in complete medium for 3 days. For in vitro experiments, OT-1 and OT-3 were added to LEC-FRC cultures (loaded or not with 1 nM OVA peptide) at different T cell/LEC-FRC ratios (1:3, 1:1, and 3:1) for 14 hours, in the presence or absence of blocking IFN-γ antibodies (10 μg/ml; XMG1.2, Bio X Cell) or granzyme-B inhibitor (300 μM; Calbiochem). For in vivo experiments, 0.05×10^6, 0.5×10^6, or 1×10^6 OT-1 cells were injected intravenously into tumor-bearing mice (day 7 or 9 after tumor inoculation).

Pmel-1 cells were loaded with 1 nM hGp100 peptide (KVPRNQDWL) (Thermo Fisher Scientific) for 1 hour in complete medium and washed with complete medium. IL-2 (50 U/ml) was added to cultures at days 2 and 4, and cells were harvested after 5 days of culture. For in vivo experiment, 12×10^6 of *Pmel-1* effector cells were injected intravenously into tumor-bearing mice (day +9 after tumor inoculation).

Polyclonal CD8$^+$ T cells were purified from spleen and LNs of C57BL/6 mice by using a CD8α$^+$ T cell isolation kit according to the manufacturer's instructions (Miltenyi Biotec). CD8$^+$ T cells were cultured with IL-2 (100 U/ml) and bone marrow–derived DCs (ratio 1:1). Before the coculture, DCs were preloaded with irradiated (100 Gy) B16F10 VC$^+$ cells (ratio of 2:1) and preactivated with lipopolysaccharide (0.1 μg/ml) for 18 hours. After 5 days of culture, CD8$^+$ T cells were harvested and adoptively transferred into tumor-bearing mice (day 10 after tumor inoculation).

IFN-γ intratumoral injection

IFN-γ (1.5 μg; PeproTech) was injected or not intratumorally twice a day for 4 days into B16F10-OVA^{+}VEGF-C^{hi} tumor-bearing mice.

Lymphatic drainage function

DC migration

Twenty microliters of 0.5-mm FITC-conjugated latex microspheres (Polysciences, diluted 1/50^{e} in PBS) was injected intratumorally. After 24 hours, flow cytometric analysis (CD11c^{+} MHCII^{+} FITC^{+}) was performed on single-cell suspensions prepared from tumor-draining inguinal and axillary LNs.

Tumor cell migration

B16F10-VEGF-C (B16-VC) melanoma cells (*31*) were stained with CTV for 20 min at 37°C in PBS, and 1×10^6 cells were injected peritumorally. Primary tumor inoculation was controlled by measuring the distance between the front leg, the back leg, and the vertebral column of the mice, and the injection was always performed at the same distances from these three locations. CTV^{+} B16-VC tumor cells were injected peritumorally at a time point primary tumor sizes were not decreased by the adoptive transfer of OT1, and the site of injection was at the limit border of the tumor mass, always in the same direction (30° related to the inguinal LN). A total of 30 μl of tumor cell suspension was injected with constant pressure (30 μl/3 s) by using a 0.3-ml syringe. After 36 hours, flow cytometric analysis (CD45^{neg} CTV^{+} GP38^{+}) was performed on single-cell suspensions prepared from tumor-draining inguinal and axillary LNs.

Metastasis quantification

Black color intensity quantification in TdLNs

The mean of black color intensity of inguinal, axillary, and brachial TdLN from pictures was calculated using ImageJ. The incidence was quantified as the percentage of black LNs among total LNs.

Gp100 staining

TdLNs (inguinal, axillary, and brachial) were mounted in OCT (Optimal cutting temperature) medium. Twenty-five–micrometer–thick sections were cut and fixed with paraformaldehyde 4% for 15 min. Slides were washed and permeabilized [PBS + 0.2% Triton X-100 + 20% dimethyl sulfoxide (DMSO); 1 hour, room temperature], and incubated for 2 hours in DMSO:H_2O_2:PBS + 0.2% Triton X-100 (1:1:4) and 1 hour in PBS + 0.2% Triton X-100 + 20% DMSO and 0.3 M glycine. After washing (PBS + 0.2% Triton X-100) and blocking (PBS + 0.2% Triton X-100 + 10% DMSO + 10% FBS), sections were stained overnight at 4°C using Alexa Fluor 647–labeled Gp100 antibody (1/200^{e}; clone; Abcam) in PBS + 5% DMSO + 5% FBS. Sections were mounted with 4′,6-diamidino-2-phenylindole (DAPI) Fluoromount-G (SouthernBiotech). Tumor area within TdLNs was detected with QuPath 0.2.3 (*69*) using intensity thresholds. This area was then normalized with the ganglion area and expressed as a percentage. LNs were considered as "metastasis-free" when the percentage was less than 0.01%. The incidence was quantified as the percentage of Gp100-positive LNs among total LNs.

Antibodies, flow cytometry, and cell sorting

Monoclonal antibodies (mAbs) used for flow cytometry are listed in Table 1 below. For flow cytometric analysis, single-cell suspensions were incubated with Fc Block (anti-CD16/32 FcγRII-RIII) for 10 min at 4°C and stained with antibodies and fixable dye for 20 to 30 min in PBS at 4°C. Intracellular staining was performed using the Intracellular Fixation and Permeabilization Buffer Set (eBioscience). For IFN-γ and granzyme-B, cells were first restimulated in complete RPMI containing phorbol 12-myristate 13-acetate (100 ng/ml; Sigma-Aldrich), ionomycin (1 μg/ml; Sigma-Aldrich), and GolgiStop solution (1/1000e; BD Biosciences) and incubated 4 hours at 37°C, 5% CO_2. Data were acquired with a Fortessa analyzer (BD) and analyzed using FlowJo software (FlowJo company). For LEC sorting from LEC/FRC cultures, cells were stained with mAbs against CD45, GP38, and CD31 and sorted using MoFlo Astrios (Beckman Coulter).

For LEC sorting from tumors, single-cell suspensions were stained with mAbs against CD45, GP38, and CD31, and LECs were sorted using a MoFlo Astrios (Beckman Coulter) as CD45^{neg}, GP38^{+}, and CD31^{+} cells. For DC sorting from tumors, single-cell suspensions were stained with mAbs against CD45, CD11c, and MHCII, and DCs were sorted using a MoFlo Astrios (Beckman Coulter) as CD45^{+}, CD11c^{+}, and MHCII^{+} cells. FMO (full stained minus one) was performed for cleaved casp-3, PD-L1, MHCII, and MHCI-OVA.

Immunohistochemistry on tumor sections

Mouse tumors were embedded for 4 hours in 4% paraformaldehyde overnight in 30% sucrose and mounted in OCT medium. Fifty-micrometer-thick sections were cut and fixed in 4% paraformaldehyde for 20 min. After washing and permeabilization [0.5% PBS/BSA + Triton X-100 (1/400e, AppliChem); 20 min, room temperature], sections were stained overnight at 4°C using a rat anti–Lyve-1 antibody (1/300e; Novus) and a rabbit anti–cleaved casp-3 (1/100e; Cell Signaling Technologies). Alexa Fluor 546–labeled goat anti-rat (1/1000e; Invitrogen) and donkey anti-rabbit AF647 (1/1000e; Jackson ImmunoResearch) and Alexa Fluor 488–labeled anti-CD45.1 (1/100e; BioLegend, clone A20) antibodies were incubated for 2 hours at room temperature. Sections were mounted with DAPI Fluoromount-G (SouthernBiotech).

Confocal imaging cytometry

Tumor lymphatic vascularization, apoptosis, and OT-1 (CD45.1) distribution in B16-OVA-VC tumors were analyzed as follows. Individual tumor slices were imaged using an upright spinning disk confocal microscope (Axio Examiner Z1 Advanced Microscope Base, Zeiss) equipped with a confocal scanner unit CSU-X1 A1 (Yokogawa Electric Corporation). Excitation of the fluorochromes was conducted via three lasers with the wavelengths of 488, 561, and 640 nm (LaserStack v4 Base, 3i). The fluorescence was detected using a 10×/0.3 numerical aperture (NA) or a 63×/1.0 NA water immersion objective (W Plan Apochromat, Zeiss), an appropriate band-pass emission filter (Semrock), and an electron-multiplying charge-coupled device camera (Evolve 512 10 MHz Back Illuminated, Photometrics). Three-dimensional image stacks were obtained by sequential acquisition of multiple field of views (FOVs) covering the whole individual section area along the complete *z* axis to screen through the complete tissue thickness using a motorized XY stage (ProScan, Prior). To ensure comparability between the samples, the same excitation light intensities and exposure times were adjusted, and the settings were chosen so that any over- or undersatured pixels were avoided. SlideBook software (6.0.17, 3i) was used for image acquisition and the creation of maximum projections. The subsequent generation of montage images from contiguous positions was performed using the Fiji "Grid/collection" stitching plugin (*70*). Before analysis, all images were processed using a "rolling ball" algorithm implemented into the Fiji plugin "Substract Background" to correct for uneven illuminated background (*71*).

Table 1. Monoclonal antibodies used for flow cytometry. Monoclonal antibodies, catalog numbers, RRID numbers, clones, and provider companies are shown. APC, allophycocyanin; PercP, peridinin-chlorophyll-protein; PE, phycoerythrine; BV 421, brilliant violet 421; BUV 395, brilliant ultra violet 395.

Supplier name	Catalog number	RRID (Research Resource Identifiers)	Clone	Provider
Brilliant Violet 510 anti-mouse CD45 antibody	103138	AB_2563061	30-F11	BioLegend
Brilliant Violet 510 anti-mouse TER-119/erythroid cell antibody	116237	AB_2561661	TER-119	BioLegend
APC anti-mouse podoplanin antibody	127410	AB_10613649	8.1.1	BioLegend
PerCP/cyanine5.5 anti-mouse CD31 antibody	102522	AB_2566761	MEC13.3	BioLegend
Pacific Blue anti-human/mouse granzyme-B antibody	515408	AB_2562196	GB11	BioLegend
Fixable viability dye eFluor 780	65-0865-18	N/A	N/A	Thermo Fisher Scientific
CD274 (PD-L1, B7-H1) monoclonal antibody, super bright 780	78-5982-82	AB_2724081	MIH5	Thermo Fisher Scientific
Ki-67 monoclonal antibody, FITC	11-5698-82	AB_11151330	SolA15	Thermo Fisher Scientific
OVA257–264 (SIINFEKL) peptide bound to H-2Kb monoclonal antibody, PE-cyanine7	25-5743-82	AB_10853347	25-D1.16	Thermo Fisher Scientific
CD45.1 monoclonal antibody (A20), PE-cyanine7	25-0453-82	AB_469629	A20	Thermo Fisher Scientific
CD11c monoclonal antibody, PE-cyanine7	25-0114-82	AB_469590	N418	Thermo Fisher Scientific
CD16/CD32 monoclonal antibody	14-0161-86	AB_467135	93	Thermo Fisher Scientific
BV421 rat anti-mouse I-A/I-E	743870	AB_2741821	2G9	BD Biosciences
PE rabbit anti-active caspase 3	550821	AB_393906	C92-605	BD Biosciences
BUV395 rat anti-mouse CD8a	563786	AB_2732919	53-6.7	BD Biosciences
Brilliant Violet 785 anti-mouse IFN-γ antibody	505838	AB_2629667	XMG1.2	BD Biosciences
BV605 rat anti-mouse CD119	745111	AB_2742716	GR20	BD Biosciences

LEC counts and cleaved casp-3 mean fluorescence intensity (MFI) in individual LEC were quantified automatically across whole tumor sections using ImageJ's (National Institutes of Health) implemented "Analyze Particles" tool upon prior intensity-based thresholding and image segmentation of individual fluorescent channels (561 nm, LEC; 640 nm, cleaved casp-3). LEC tumor distribution was calculated as the ratio of the shortest distance of individual LECs to the tumor edge divided by the sum of individual LEC distances toward the center and the edge of the tumor. Distance analysis between individual OT-1 and LEC and the verification of nonrandomized distribution pattern was performed using ImageJ's plugin DiAna (*72*).

Live cell imaging

LECs from WT (LC3-GFP) and β_2m^{KO} LEC/FRC cocultures were sorted by flow cytometry (see the "Antibodies, flow cytometry, and cell sorting" section), and 5×10^4 cells (ratio 1:1) were plated on fibronectin/PureCol-coated 35-mm by 10-mm petri dish. One day later, cells were loaded with OVA peptide (SIINFEKL) (1 nM; Sigma-Aldrich) and stained with 0.5 μM eF(eFluor)670-labeled cell proliferation dye (eBioscience) for 30 min at 37°C in PBS. Cells were washed three times in PBS and incubated for 30 min at 37°C with NucView 405 casp-3 substrate (5 μM; Biotium). After washing, 1×10^6 in vitro activated OT-1 cells were added to the cultures. Time-lapse confocal spinning disk video microscopy was performed to measure cleaved casp-3 MFI in individual LEC as described above. To detect and to quantify LEC-touching OT-1 number, a mask around individual LECs was generated using the all-LEC channel. Last, this mask was applied to the bright-field channel to count temporal contacts between OT-1 and WT or β_2m^{KO} at a time-lapse interval of 1 min over 270 min.

RNA isolation and reverse transcription qPCR

Total RNA was isolated using the RNeasy Plus Micro Kit (QIAGEN) from sorted LEC and DC (see the "Antibodies, flow cytometry, and cell sorting" section). cDNA was synthesized using the PrimeScript RT Reagent Kit followed by a preamplification of the respective genes of interest using the TaqMan Preamp Master Mix (Applied

Biosystems). PCRs were performed with the ABI Prism 7900 HT detection system and the PowerUp SYBR Green Master Mix (Applied Biosystems). Results (two replicates) were normalized with glyceraldehyde phosphate dehydrogenase (gapdh), and l32 normalization factors and fold changes were calculated according to the GeNorm method.

Primers were as follows: *Ifngr2*: GGCTGGAGCCATTTCAACAC (forward) and AAAGGGCCTTCAACCTGTTC (reverse); *Ifngr1*: GCCTAAAGGGAAAGGTCGGG (forward) and CACTCCGGTTATGCTCCACA (reverse); *Jak1*: GTGCGTTTTTAGAGCGCAGG (forward) and CAGAGCTGATCACTTCCGTGT (reverse); *Stat1*: AAAGTCATGGCTGCCGAGAA (forward) and CATCGGTTCTGGTGCTTCCT (reverse); *Irf1*: CCATTCACACAGGCCGATAC (forward) and ACAGCAGAGCTGCCCTTGTT (reverse); *C2ta*: CCCTGCGTGTGATGGATGTC (forward) and ATCTCAGACTGATCCTGGCAT (reverse); *H2-ab*: CTGTGGTGG TGCTGATGG T (forward) and CGTTGGTGAAGTAGCACTCG (reverse); *Cd274*: CATCCCAGAACTGCCTGCAA (forward) and TGCCAATCGACGATCAGAGG (reverse); *H2kb*: GTGATCTCTGGCTGTGAAGT (forward) and GTCTCCACAAGCTCCATGTC (reverse); *Nlrc5*: CTTCCCGCCTCTCCTTCCACAAT (forward) and CTCCACCTGCCCACATCCTACCA (reverse); *Tap1*: GGACTTGCCTTGTTCCGAGAG (forward) and GCTGCCACATAACTGATAGCGA (reverse); *Lmp2*: CATGAACCGAGATGGCTCTAGT (forward) and TCATCGTAGAATTTTGGCAGCTC (reverse); *B2m*: CCCCACTGAGACTGATACATACG (forward) and CGATCCCAGTAGACGGTCTTG (reverse); *Gapdh*: CCCGTAGACAAAATGGTGAAG (forward) and AGGTCAATGAAGGGGTCGTTG (reverse); and *L32*: GAAACTGGCGGAAACCCA (forward) and GGATCTGGCCCTTGAACCTT (reverse). For VEGF-C qPCR, a RT2 qPCR primer assay was used (QIAGEN, catalog no 330001 PPM03061F; reference position: 449).

Statistical analysis

Statistical analysis was performed with Prism (version 9.0; GraphPad, San Diego, CA). Groups were first compared with *F* test to test the hypothesis of equal variances. In the presence of significantly different variances, datasets were compared using either a nonparametric test (specifically Mann-Whitney test for comparison of two groups). In the presence of equal variances, parametric tests were used, specifically one-way analysis of variance (ANOVA) with Tukey's multiple comparisons test for comparison of three or more groups and two-way ANOVA with Sidak's multiple comparisons test for comparison of the dataset containing repeated measurements. *P* values were reported as follows: $*P < 0.05$, $**P < 0.01$, $***P < 0.001$, and $****P < 0.0001$. Some data points were omitted from analysis by identifying outliers with the Prism software (ROUT method).

SUPPLEMENTARY MATERIALS

Supplementary material for this article is available at https://science.org/doi/10.1126/sciadv.abl5162

View/request a protocol for this paper from *Bio-protocol*.

REFERENCES AND NOTES

1. S. P. Leong, E. K. Nakakura, R. Pollock, M. A. Choti, D. L. Morton, W. D. Henner, A. Lal, R. Pillai, O. H. Clark, B. Cady, Unique patterns of metastases in common and rare types of malignancy. *J. Surg. Oncol.* **103**, 607–614 (2011).
2. S. A. Stacker, S. P. Williams, T. Karnezis, R. Shayan, S. B. Fox, M. G. Achen, Lymphangiogenesis and lymphatic vessel remodelling in cancer. *Nat. Rev. Cancer* **14**, 159–172 (2014).
3. M. Brown, F. P. Assen, A. Leithner, J. Abe, H. Schachner, G. Asfour, Z. Bago-Horvath, J. V. Stein, P. Uhrin, M. Sixt, D. Kerjaschki, Lymph node blood vessels provide exit routes for metastatic tumor cell dissemination in mice. *Science* **359**, 1408–1411 (2018).
4. E. R. Pereira, D. Kedrin, G. Seano, O. Gautier, E. F. J. Meijer, D. Jones, S.-M. Chin, S. Kitahara, E. M. Bouta, J. Chang, E. Beech, H.-S. Jeong, M. C. Carroll, A. G. Taghian, T. P. Padera, Lymph node metastases can invade local blood vessels, exit the node, and colonize distant organs in mice. *Science* **359**, 1403–1407 (2018).
5. S. S. Dadras, T. Paul, J. Bertoncini, L. F. Brown, A. Muzikansky, D. G. Jackson, U. Ellwanger, C. Garbe, M. C. Mihm, M. Detmar, Tumor lymphangiogenesis: A novel prognostic indicator for cutaneous melanoma metastasis and survival. *Am. J. Pathol.* **162**, 1951–1960 (2003).
6. M. Rinderknecht, M. Detmar, Tumor lymphangiogenesis and melanoma metastasis. *J. Cell. Physiol.* **216**, 347–354 (2008).
7. W. Thiele, J. P. Sleeman, Tumor-induced lymphangiogenesis: A target for cancer therapy? *J. Biotechnol.* **124**, 224–241 (2006).
8. J. B. Burton, S. J. Priceman, J. L. Sung, E. Brakenhielm, D. S. An, B. Pytowski, K. Alitalo, L. Wu, Suppression of prostate cancer nodal and systemic metastasis by blockade of the lymphangiogenic axis. *Cancer Res.* **68**, 7828–7837 (2008).
9. A. Gogineni, M. Caunt, A. Crow, C. V. Lee, G. Fuh, N. van Bruggen, W. Ye, R. M. Weimer, Inhibition of VEGF-C modulates distal lymphatic remodeling and secondary metastasis. *PLOS ONE* **8**, e68755 (2013).
10. S. Hirakawa, L. F. Brown, S. Kodama, K. Paavonen, K. Alitalo, M. Detmar, VEGF-C-induced lymphangiogenesis in sentinel lymph nodes promotes tumor metastasis to distant sites. *Blood* **109**, 1010–1017 (2007).
11. T. Hoshida, N. Isaka, J. Hagendoorn, E. di Tomaso, Y. L. Chen, B. Pytowski, D. Fukumura, T. P. Padera, R. K. Jain, Imaging steps of lymphatic metastasis reveals that vascular endothelial growth factor-C increases metastasis by increasing delivery of cancer cells to lymph nodes: Therapeutic implications. *Cancer Res.* **66**, 8065–8075 (2006).
12. J. Lin, A. S. Lalani, T. C. Harding, M. Gonzalez, W.-W. Wu, B. Luan, G. H. Tu, K. Koprivnikar, M. J. VanRoey, Y. He, K. Alitalo, K. Jooss, Inhibition of lymphogenous metastasis using adeno-associated virus-mediated gene transfer of a soluble VEGFR-3 decoy receptor. *Cancer Res.* **65**, 6901–6909 (2005).
13. S. J. Mandriota, L. Jussila, M. Jeltsch, A. Compagni, D. Baetens, R. Prevo, S. Banerji, J. Huarte, R. Montesano, D. G. Jackson, L. Orci, K. Alitalo, G. Christofori, M. S. Pepper, Vascular endothelial growth factor-C-mediated lymphangiogenesis promotes tumour metastasis. *EMBO J.* **20**, 672–682 (2001).
14. N. Roberts, B. Kloos, M. Cassella, S. Podgrabinska, K. Persaud, Y. Wu, B. Pytowski, M. Skobe, Inhibition of VEGFR-3 activation with the antagonistic antibody more potently suppresses lymph node and distant metastases than inactivation of VEGFR-2. *Cancer Res.* **66**, 2650–2657 (2006).
15. M. Skobe, T. Hawighorst, D. G. Jackson, R. Prevo, L. Janes, P. Velasco, L. Riccardi, K. Alitalo, K. Claffey, M. Detmar, Induction of tumor lymphangiogenesis by VEGF-C promotes breast cancer metastasis. *Nat. Med.* **7**, 192–198 (2001).
16. S. A. Stacker, C. Caesar, M. E. Baldwin, G. E. Thornton, R. A. Williams, R. Prevo, D. G. Jackson, S. I. Nishikawa, H. Kubo, M. G. Achen, VEGF-D promotes the metastatic spread of tumor cells via the lymphatics. *Nat. Med.* **7**, 186–191 (2001).
17. S. Hirakawa, S. Kodama, R. Kunstfeld, K. Kajiya, L. F. Brown, M. Detmar, VEGF-A induces tumor and sentinel lymph node lymphangiogenesis and promotes lymphatic metastasis. *J. Exp. Med.* **201**, 1089–1099 (2005).
18. C. N. Qian, B. Berghuis, G. Tsarfaty, M. Bruch, E. J. Kort, J. Ditlev, I. Tsarfaty, E. Hudson, D. G. Jackson, D. Petillo, J. Chen, J. H. Resau, B. T. Teh, Preparing the "soil": The primary tumor induces vasculature reorganization in the sentinel lymph node before the arrival of metastatic cancer cells. *Cancer Res.* **66**, 10365–10376 (2006).
19. M. Kim, Y. J. Koh, K. E. Kim, B. I. Koh, D. H. Nam, K. Alitalo, I. Kim, G. Y. Koh, CXCR4 signaling regulates metastasis of chemoresistant melanoma cells by a lymphatic metastatic niche. *Cancer Res.* **70**, 10411–10421 (2010).
20. Q. Ma, L. C. Dieterich, K. Ikenberg, S. B. Bachmann, J. Mangana, S. T. Proulx, V. C. Amann, M. P. Levesque, R. Dummer, P. Baluk, D. M. McDonald, M. Detmar, Unexpected contribution of lymphatic vessels to promotion of distant metastatic tumor spread. *Sci. Adv.* **4**, eaat4758 (2018).
21. M. A. S. Broggi, L. Maillat, C. C. Clement, N. Bordry, P. Corthésy, A. Auger, M. Matter, R. Hamelin, L. Potin, D. Demurtas, E. Romano, A. Harari, D. E. Speiser, L. Santambrogio, M. A. Swartz, Tumor-associated factors are enriched in lymphatic exudate compared to plasma in metastatic melanoma patients. *J. Exp. Med.* **216**, 1091–1107 (2019).
22. J. D. Peske, E. D. Thompson, L. Gemta, R. A. Baylis, Y. X. Fu, V. H. Engelhard, Effector lymphocyte-induced lymph node-like vasculature enables naive T-cell entry into tumours and enhanced anti-tumour immunity. *Nat. Commun.* **6**, 7114 (2015).
23. E. D. Thompson, H. L. Enriquez, Y. X. Fu, V. H. Engelhard, Tumor masses support naive T cell infiltration, activation, and differentiation into effectors. *J. Exp. Med.* **207**, 1791–1804 (2010).
24. P. Yu, Y. Lee, W. Liu, R. K. Chin, J. Wang, Y. Wang, A. Schietinger, M. Philip, H. Schreiber, Y. X. Fu, Priming of naive T cells inside tumors leads to eradication of established tumors. *Nat. Immunol.* **5**, 141–149 (2004).

25. A. W. Lund, M. Wagner, M. Fankhauser, E. S. Steinskog, M. A. Broggi, S. Spranger, T. F. Gajewski, K. Alitalo, H. P. Eikesdal, H. Wiig, M. A. Swartz, Lymphatic vessels regulate immune microenvironments in human and murine melanoma. *J. Clin. Invest.* **126**, 3389–3402 (2016).
26. E. W. Roberts, M. L. Broz, M. Binnewies, M. B. Headley, A. E. Nelson, D. M. Wolf, T. Kaisho, D. Bogunovic, N. Bhardwaj, M. F. Krummel, Critical role for $CD103^+/CD141^+$ dendritic cells bearing CCR7 for tumor antigen trafficking and priming of T cell immunity in melanoma. *Cancer Cell* **30**, 324–336 (2016).
27. N. Bordry, M. A. S. Broggi, K. de Jonge, K. Schaeuble, P. O. Gannon, P. G. Foukas, E. Danenberg, E. Romano, P. Baumgaertner, M. Fankhauser, N. Wald, L. Cagnon, S. Abed-Maillard, H. M. E. Hajjami, T. Murray, K. Ioannidou, I. Letovanec, P. Yan, O. Michielin, M. Matter, M. A. Swartz, D. E. Speiser, Lymphatic vessel density is associated with $CD8^+$ T cell infiltration and immunosuppressive factors in human melanoma. *Onco. Targets. Ther.* **7**, e1462878 (2018).
28. M. Fankhauser, M. A. S. Broggi, L. Potin, N. Bordry, L. Jeanbart, A. W. Lund, E. da Costa, S. Hauert, M. Rincon-Restrepo, C. Tremblay, E. Cabello, K. Homicsko, O. Michielin, D. Hanahan, D. E. Speiser, M. A. Swartz, Tumor lymphangiogenesis promotes T cell infiltration and potentiates immunotherapy in melanoma. *Sci. Transl. Med.* **9**, eaal4712 (2017).
29. B. Mlecnik, G. Bindea, A. Kirilovsky, H. K. Angell, A. C. Obenauf, M. Tosolini, S. E. Church, P. Maby, A. Vasaturo, M. Angelova, T. Fredriksen, S. Mauger, M. Waldner, A. Berger, M. R. Speicher, F. Pagès, V. Valge-Archer, J. Galon, The tumor microenvironment and Immunoscore are critical determinants of dissemination to distant metastasis. *Sci. Transl. Med.* **8**, 327ra26 (2016).
30. T. Kimura, M. Sugaya, T. Oka, A. Blauvelt, H. Okochi, S. Sato, Lymphatic dysfunction attenuates tumor immunity through impaired antigen presentation. *Oncotarget* **6**, 18081–18093 (2015).
31. A. W. Lund, F. V. Duraes, S. Hirosue, V. R. Raghavan, C. Nembrini, S. N. Thomas, A. Issa, S. Hugues, M. A. Swartz, VEGF-C promotes immune tolerance in B16 melanomas and cross-presentation of tumor antigen by lymph node lymphatics. *Cell Rep.* **1**, 191–199 (2012).
32. C. Tacconi, F. Ungaro, C. Correale, V. Arena, L. Massimino, M. Detmar, A. Spinelli, M. Carvello, M. Mazzone, A. I. Oliveira, F. Rubbino, V. Garlatti, S. Spanò, E. Lugli, F. S. Colombo, A. Malesci, L. Peyrin-Biroulet, S. Vetrano, S. Danese, S. D'Alessio, Activation of the VEGFC/VEGFR3 pathway induces tumor immune escape in colorectal cancer. *Cancer Res.* **79**, 4196–4210 (2019).
33. L. C. Dieterich, K. Ikenberg, T. Cetintas, K. Kapaklikaya, C. Hutmacher, M. Detmar, Tumor-associated lymphatic vessels upregulate PDL1 to inhibit T-cell activation. *Front. Immunol.* **8**, 66 (2017).
34. R. S. Lane, J. Femel, A. P. Breazeale, C. P. Loo, G. Thibault, A. Kaempf, M. Mori, T. Tsujikawa, Y. H. Chang, A. W. Lund, IFNγ-activated dermal lymphatic vessels inhibit cytotoxic T cells in melanoma and inflamed skin. *J. Exp. Med.* **215**, 3057–3074 (2018).
35. A. O. Gkountidi, L. Garnier, J. Dubrot, J. Angelillo, G. Harlé, D. Brighouse, L. J. Wrobel, R. Pick, C. Scheiermann, M. A. Swartz, S. Hugues, MHC class II antigen presentation by lymphatic endothelial cells in tumors promotes intratumoral regulatory T cell-suppressive functions. *Cancer Immunol. Res.* **9**, 748–764 (2021).
36. E. Song, T. Mao, H. Dong, L. S. B. Boisserand, S. Antila, M. Bosenberg, K. Alitalo, J.-L. Thomas, A. Iwasaki, VEGF-C-driven lymphatic drainage enables immunosurveillance of brain tumours. *Nature* **577**, 689–694 (2020).
37. M. S. Sasso, N. Mitrousis, Y. Wang, P. S. Briquez, S. Hauert, J. Ishihara, J. A. Hubbell, M. A. Swartz, Lymphangiogenesis-inducing vaccines elicit potent and long-lasting T cell immunity against melanomas. *Sci. Adv.* **7**, eabe4362 (2021).
38. M. T. Spiotto, D. A. Rowley, H. Schreiber, Bystander elimination of antigen loss variants in established tumors. *Nat. Med.* **10**, 294–298 (2004).
39. M. T. Spiotto, H. Schreiber, Rapid destruction of the tumor microenvironment by CTLs recognizing cancer-specific antigens cross-presented by stromal cells. *Cancer Immun.* **5**, 8 (2005).
40. B. Zhang, N. A. Bowerman, J. K. Salama, H. Schmidt, M. T. Spiotto, A. Schietinger, P. Yu, Y. X. Fu, R. R. Weichselbaum, D. A. Rowley, D. M. Kranz, H. Schreiber, Induced sensitization of tumor stroma leads to eradication of established cancer by T cells. *J. Exp. Med.* **204**, 49–55 (2007).
41. J. J. Listopad, T. Kammertoens, K. Anders, B. Silkenstedt, G. Willimsky, K. Schmidt, A. A. Kuehl, C. Loddenkemper, T. Blankenstein, Fas expression by tumor stroma is required for cancer eradication. *Proc. Natl. Acad. Sci. U.S.A.* **110**, 2276–2281 (2013).
42. T. Schuler, T. Blankenstein, Cutting edge: CD8+ effector T cells reject tumors by direct antigen recognition but indirect action on host cells. *J. Immunol.* **170**, 4427–4431 (2003).
43. B. Zhang, T. Karrison, D. A. Rowley, H. Schreiber, IFN-γ– and TNF-dependent bystander eradication of antigen-loss variants in established mouse cancers. *J. Clin. Invest.* **118**, 1398–1404 (2008).
44. Z. Qin, J. Schwartzkopff, F. Pradera, T. Kammertoens, B. Seliger, H. Pircher, T. Blankenstein, A critical requirement of interferon gamma-mediated angiostasis for tumor rejection by $CD8^+$ T cells. *Cancer Res.* **63**, 4095–4100 (2003).
45. T. Kammertoens, C. Friese, A. Arina, C. Idel, D. Briesemeister, M. Rothe, A. Ivanov, A. Szymborska, G. Patone, S. Kunz, D. Sommermeyer, B. Engels, M. Leisegang, A. Textor, H. J. Fehling, M. Fruttiger, M. Lohoff, A. Herrmann, H. Yu, R. Weichselbaum, W. Uckert, N. Hübner, H. Gerhardt, D. Beule, H. Schreiber, T. Blankenstein, Tumour ischaemia by interferon-γ resembles physiological blood vessel regression. *Nature* **545**, 98–102 (2017).
46. R. P. Kataru, H. Kim, C. Jang, D. K. Choi, B. I. Koh, M. Kim, S. Gollamudi, Y.-K. Kim, S.-H. Lee, G. Y. Koh, T lymphocytes negatively regulate lymph node lymphatic vessel formation. *Immunity* **34**, 96–107 (2011).
47. E. Bazigou, O. T. A. Lyons, A. Smith, G. E. Venn, C. Cope, N. A. Brown, T. Makinen, Genes regulating lymphangiogenesis control venous valve formation and maintenance in mice. *J. Clin. Invest.* **121**, 2984–2992 (2011).
48. H. M. Lee, A. Fleige, R. Forman, S. Cho, A. A. Khan, L.-L. Lin, D. T. Nguyen, A. O'Hara-Hall, Z. Yin, C. A. Hunter, W. Muller, L.-F. Lu, IFNγ signaling endows DCs with the capacity to control type I inflammation during parasitic infection through promoting $T\text{-}bet^+$ regulatory T cells. *PLOS Pathog.* **11**, e1004635 (2015).
49. G. P. Dunn, C. M. Koebel, R. D. Schreiber, Interferons, immunity and cancer immunoediting. *Nat. Rev. Immunol.* **6**, 836–848 (2006).
50. A. J. Ligocki, J. R. Brown, J. Y. Niederkorn, Role of interferon-γ and cytotoxic T lymphocytes in intraocular tumor rejection. *J. Leukoc. Biol.* **99**, 735–747 (2016).
51. J. Zhou, P. Ma, J. Li, X. Cui, W. Song, Improvement of the cytotoxic T lymphocyte response against hepatocellular carcinoma by transduction of cancer cells with an adeno-associated virus carrying the interferon-γ gene. *Mol. Med. Rep.* **13**, 3197–3205 (2016).
52. G. Segal, S. Prato, D. Zehn, J. D. Mintern, J. A. Villadangos, Target density, not affinity or avidity of antigen recognition, determines adoptive T cell therapy outcomes in a mouse lymphoma model. *J. Immunol.* **196**, 3935–3942 (2016).
53. S. Hirosue, E. Vokali, V. R. Raghavan, M. Rincon-Restrepo, A. W. Lund, P. Corthésy-Henrioud, F. Capotosti, C. Halin Winter, S. Hugues, M. A. Swartz, Steady-state antigen scavenging, cross-presentation, and $CD8^+$ T cell priming: A new role for lymphatic endothelial cells. *J. Immunol.* **192**, 5002–5011 (2014).
54. N. Cousin, S. Cap, M. Dihr, C. Tacconi, M. Detmar, L. C. Dieterich, Lymphatic PD-L1 expression restricts tumor-specific $CD8^+$ T cell responses. *Cancer Res.* **81**, 4133–4144 (2021).
55. U. Blohm, D. Potthoff, A. J. van der Kogel, H. Pircher, Solid tumors "melt" from the inside after successful CD8 T cell attack. *Eur. J. Immunol.* **36**, 468–477 (2006).
56. A. Schurich, J. P. Böttcher, S. Burgdorf, P. Penzler, S. Hegenbarth, M. Kern, A. Dolf, E. Endl, J. Schultze, E. Wiertz, D. Stabenow, C. Kurts, P. Knolle, Distinct kinetics and dynamics of cross-presentation in liver sinusoidal endothelial cells compared to dendritic cells. *Hepatology* **50**, 909–919 (2009).
57. N. von Oppen, A. Schurich, S. Hegenbarth, D. Stabenow, R. Tolba, R. Weiskirchen, A. Geerts, W. Kolanus, P. Knolle, L. Diehl, Systemic antigen cross-presented by liver sinusoidal endothelial cells induces liver-specific CD8 T-cell retention and tolerization. *Hepatology* **49**, 1664–1672 (2009).
58. T. Makinen, T. Veikkola, S. Mustjoki, T. Karpanen, B. Catimel, E. C. Nice, L. Wise, A. Mercer, H. Kowalski, D. Kerjaschki, S. A. Stacker, M. G. Achen, K. Alitalo, Isolated lymphatic endothelial cells transduce growth, survival and migratory signals via the VEGF-C/D receptor VEGFR-3. *EMBO J.* **20**, 4762–4773 (2001).
59. B. Engels, V. H. Engelhard, J. Sidney, A. Sette, D. C. Binder, R. B. Liu, D. M. Kranz, S. C. Meredith, D. A. Rowley, H. Schreiber, Relapse or eradication of cancer is predicted by peptide-major histocompatibility complex affinity. *Cancer Cell* **23**, 516–526 (2013).
60. L. Ni, J. Lu, Interferon gamma in cancer immunotherapy. *Cancer Med.* **7**, 4509–4516 (2018).
61. S. J. Patel, N. E. Sanjana, R. J. Kishton, A. Eidizadeh, S. K. Vodnala, M. Cam, J. J. Gartner, L. Jia, S. M. Steinberg, T. N. Yamamoto, A. S. Merchant, G. U. Mehta, A. Chichura, O. Shalem, E. Tran, R. Eil, M. Sukumar, E. P. Guijarro, C.-P. Day, P. Robbins, S. Feldman, G. Merlino, F. Zhang, N. P. Restifo, Identification of essential genes for cancer immunotherapy. *Nature* **548**, 537–542 (2017).
62. K. S. Kobayashi, P. J. van den Elsen, NLRC5: A key regulator of MHC class I-dependent immune responses. *Nat. Rev. Immunol.* **12**, 813–820 (2012).
63. L. Martinez-Lostao, A. Anel, J. Pardo, How do cytotoxic lymphocytes kill cancer cells? *Clin. Cancer Res.* **21**, 5047–5056 (2015).
64. B. H. Koller, P. Marrack, J. W. Kappler, O. Smithies, Normal development of mice deficient in β_2M, MCClass I proteins, and $CD8^+$ T cells. *Science* **248**, 1227–1230 (1990).
65. S. Enouz, L. Carrié, D. Merkler, M. J. Bevan, D. Zehn, Autoreactive T cells bypass negative selection and respond to self-antigen stimulation during infection. *J. Exp. Med.* **209**, 1769–1779 (2012).
66. W. W. Overwijk, M. R. Theoret, S. E. Finkelstein, D. R. Surman, L. A. de Jong, F. A. Vyth-Dreese, T. A. Dellemijn, P. A. Antony, P. J. Spiess, D. C. Palmer, D. M. Heimann, C. A. Klebanoff, Z. Yu, L. N. Hwang, L. Feigenbaum, A. M. Kruisbeek, S. A. Rosenberg, N. P. Restifo, Tumor regression and autoimmunity after reversal of a functionally tolerant state of self-reactive $CD8^+$ T cells. *J. Exp. Med.* **198**, 569–580 (2003).
67. N. Mizushima, A. Yamamoto, M. Matsui, T. Yoshimori, Y. Ohsumi, In vivo analysis of autophagy in response to nutrient starvation using transgenic mice expressing a fluorescent autophagosome marker. *Mol. Biol. Cell* **15**, 1101–1111 (2004).

68. A. L. Fletcher, V. Lukacs-Kornek, E. D. Reynoso, S. E. Pinner, A. Bellemare-Pelletier, M. S. Curry, A. R. Collier, R. L. Boyd, S. J. Turley, Lymph node fibroblastic reticular cells directly present peripheral tissue antigen under steady-state and inflammatory conditions. *J. Exp. Med.* **207**, 689–697 (2010).
69. P. Bankhead, M. B. Loughrey, J. A. Fernández, Y. Dombrowski, D. G. McArt, P. D. Dunne, S. McQuaid, R. T. Gray, L. J. Murray, H. G. Coleman, J. A. James, M. Salto-Tellez, P. W. Hamilton, QuPath: Open source software for digital pathology image analysis. *Sci. Rep.* **7**, 16878 (2017).
70. S. Preibisch, S. Saalfeld, P. Tomancak, Globally optimal stitching of tiled 3D microscopic image acquisitions. *Bioinformatics* **25**, 1463–1465 (2009).
71. S. Sternberg, Biomedical image processing. *Computer* **16**, 22–34 (1983).
72. J. F. Gilles, M. Dos Santos, T. Boudier, S. Bolte, N. Heck, DiAna, an ImageJ tool for object-based 3D co-localization and distance analysis. *Methods* **115**, 55–64 (2017).

Acknowledgments: We thank J. P. Aubry-Lachainaye, C. Gameiro, and G. Schneiter for excellent assistance in flow cytometry; N. Liaudet and F. Prodon for excellent assistance in imaging; D. Chollet for excellent assistance in qPCR experiments; E. Cosset for the generation of MC38-OVA-VEGF-C^{hi} cells; J. Angelillo for the color intensity quantification in TdLNs; B. Kizil and I. Senoner for the setup of Gp100 immunofluorescent staining; D. Speiser and K. Schäuble for helpful discussion; W. Muller for providing IFN-γ^{fifl} mice; and P. Romero for providing OT-3 mice. **Funding:** This work was supported by the Geneva Cancer League to S.H., the Swiss Cancer League (KLS-4836-08-2019) to C.S., and the Swiss National Science Foundation (310030_16654 and 310030_185255 to S.H. and 310030_182417/1 to C.S.). **Author contributions:** Conceptualization: L.G. and S.H. Methodology: L.G., R.P., J.M., C.S., M.S., J.B.-L., N.L., and S.H. Investigation: L.G., R.P., J.M., M.S., D.B., T.K., T.B., N.P., N.L.T., T.V.P., D.M., C.S., and S.H. Visualization: L.G., R.P., J.M., M.S., D.B., N.P., T.V.P., D.M., C.S., and S.H. Supervision: L.G. and S.H. Writing—Original draft: L.G. and S.H. Writing—Review and editing: L.G., R.P., S.H., C.S., T.K., N.L.T., and T.B. Resources: C.S. and S.H. **Competing interests:** The authors declare that they have no competing interests. **Data and materials availability:** The data underlying this article are accessible at https://doi.org/10.26037/yareta:w7bzl7vlhbfanbfgzmsifu33p4. All data needed to evaluate the conclusions in the paper are present in the paper and/or the Supplementary Materials.

Submitted 19 July 2021
Accepted 22 April 2022
Published 8 June 2022
10.1126/sciadv.abl5162